이학박사학위논문

Electromagnetic Absorption and Gas Barrier Properties of Large-Area Graphene for Smart Applications

대면적 그래핀의 전자기파 흡수 및 가스 배리어 특성과 스마트 어플리케이션에의 응용 연구

2019 년 2 월

서울대학교 대학원

화학부 물리화학 전공

이 상 규

Electromagnetic Absorption and Gas Barrier Properties of Large-Area Graphene for Smart Applications

대면적 그래핀의 전자기파 흡수 및 가스 배리어 특성과 스마트 어플리케이션에의 응용 연구

지도교수: 홍 병 희

이 논문을 이학박사 학위논문으로 제출함

2019년 2월

서울대학교 대학원

화학부 물리화학 전공

이 상 규

이상규의 이학박사 학위논문을 인준함

2018년 12월 9일

위 원 장 장 두 전

부위원장 홍 병 희

위 원 남 좌 민

위 원 조 성 표

위 원 박 수 범

Ph.D. Thesis

Electromagnetic Absorption and Gas Barrier Properties of Large-Area Graphene for Smart Applications

Supervisor: Professor Byung Hee Hong

Major: Physical Chemistry

By Sang Kyu Lee

Department of Chemistry

Graduate School of Seoul National University

2019

Abstract

Graphene is an atomically thin carbon material with a two-dimensional hexagonal lattice that shows outstanding electrical and mechanical properties as well as excellent biocompatibility.

Thanks to its outstanding electrical property, graphene can be utilized as very high performance electromagnetic (EM) wave shielding materials with extreme thin and transparent, light-weight. It is reported that ideal graphene can block as much as 97.8% of EMI. Also, It is reported that the monolayer graphene synthesized by CVD has an average SE value of 2.27dB, corresponding to 40% shielding, presenting 7 times (in terms of dB) greater SE than gold film. In addition, small gas molecules cannot pass through graphene, because its densely packed hexagonal lattice structure of carbon atoms. In these reasons, I believe that graphene is the most suitable materials to realize such smart electronics (wearable contact lens device, heater for automobile, so on)

We report a CVD graphene-based highly conducting contact lens platform that reduces the exposure to EM waves and dehydration. Additionally, we demonstrate simple contact lens platform micro LED operating devices fabricated by CVD graphene-based conductive layers. Thus, we believe that the graphene-coated contact lens would provide a healthcare and bionic platform for wearable technologies in the future. We also demonstrate EM wave shielding mechanism of graphene. Graphene

generate a heat energy as a result of EM wave shielding. Therefore, this allows graphene heater to be used widely in fields of automobile defogging/deicing systems, smart heating windows and EM-wave detecting sensors.

Keyword : graphene EMI shielding, graphene WVTR, graphene contact lens, graphene heat, graphene diamagnetism

Student Number : 2014-31011

Contents

List of Figures

Chapter 1

Figure 5. Overview of Applications of Graphene in different sectors ranging from conductive ink to chemical sensors, light emitting devices, composites, energy, touch panels and high frequency electronics. [Adapted from Ref. 13]

Figure 6. The contact lens sensor under co-development by Google and Novartis. It measures glucose concentration in tears using a miniaturized electrochemical sensor embedded into a hydrogel matrix. a) A schematic of the contact lens sensor, showing the electrical circuitry of the sensing system. b) The contact lens sensor prototype. c) The wireless chip, which is mounted, with the sensor, onto an electronic ring, and then embedded into the contact lens. [Adapted From 17] Copyright 2014, Google X.

Figure 7. Micromechanical exfoliation of graphene. (a) Adhesive tape is pressed against a graphene. (b) Few layers of graphene are attached to the tape. (c) The tape with layers of graphene is pressed against a surface of target substrate. (d) Upon peeling off, the bottom layer is left on the substrate. [Adapted from Ref. 18]

Figure 8. GO synthesis and reduction. Graphite can be oxidized with different procedures in the presence of strong acids. The GO flakes have the basal plane functionalized with epoxy and hydroxyl groups, both above and below it, and the edges with a variety of functional groups. This makes GO sheets defective. A partial restoration of the electronic properties is obtainable following different reduction strategies. [Adapted from Ref. 19]

Figure 9. (a) Growth of epitaxial graphene on silicon carbide wafer via sublimation of silicon atoms [Adapted from Ref. 20]. (b) Top view of covalently bound stretched graphene (CSG) model on SiC(0001). (c) graphene on bulk-truncated SiC(0001) surface [Adapted from ref. 21]

Figure 10. Growth kinetics in CVD-produced graphene on various catalysts: Case of CH4 on Ni and Cu. [Adapted from Ref. 22]

Figure 11. The process flow associated with the transfer of CVD-grown graphene onto SiO2. (i) one side of the graphene-covered copper foil is spin-coated with PMMA (950K A2), (ii) the PMMA is cured at 110 °C for 15 s on a hot plate, (iii) a diluted nitric acid solution (5 mL HNO3, 15 mL water) is used to etch away the graphene on the side of the copper foil that is not covered by PMMA, and (iv) a 1 M solution of ammonium persulfate is utilized at 70 °C to etch away the copper foil, leaving behind a strip of PMMA covered with CVDgrown graphene on one side. Subsequently, the PMMA strip is placed on a clean SiO2 wafer piece, and the PMMA is removed via dipping the sample into acetone. [Adapted from Ref. 26]

Figure 12. Roll to roll production of graphene and touch screen application. (a) Schematic of the roll-based production of graphene films grown on a copper foil. The process includes adhesion of polymer support such as thermal release tape, copper etching (rinsing) and dry-transfer-printing on a target substrate. (b-d) Photographs of application of graphene films grown by roll-to-roll method. (b) Screen printing process of silver paste electrodes on graphene/poly(ethylene terephthalate) (PET) films. The inset shows 3.1-inch graphene/PET panels patterned with silver electrodes before assembly. (c) An assembled graphene/PET touch panel showing outstanding _exibility. (d) A graphene-based touch-screen panel connected to a computer with control software. [Adapted from Ref. 27]

Chapter 2

Figure 1. Schematic working principle of a graphene-coated contact lens and its fabrication process. (a) Electromagnetic (EM) wave passes through contact lens and absorbed by an eyeball, possibly causing heat damage inside. **(b)** EM energy is absorbed by graphene and disscipated as a heat before reaching the interior of the eye. **(c-d)** Dehydration of a contact lens can be reduced due to the gas-impermeability of graphene **(e)** The fabrication process of the graphene-coated contact lens.

Figure 2. Optical and electrical properties of graphene films. **(a)** Optical and SEM images of graphene samples transferred on a SiO_2 substrate. **(b)** Raman spectrum of graphene showing monolayer thickness and low defect density. **(c)** Transmittance of a bare contact lens and a graphene-coated contact lens. Scale bar: 1cm. **(d-f)** Evaluation of electrical properties of graphene samples, including 4-point sheet resistance masurement and *I-V* characteristics.

Figure 3. EMI shielding effect of the graphene-coated contact lens tested in a microwave oven. (a) Sample prapration for the microwave oven test. Egg whites on a Si wafer are covered with the contact lenses with and without graphene coating, respectively. **(b)** A microwave oven test showing the excellent EMI shielding effect of the graphene-coated contact lens. The egg white protected by graphene shows less thermal denaturalization. **(c)** IR camera images showing the the elevated temperature of the graphene-coated

lens inside a microwave oven, indicating the EM energy is efficiently absorbed and dissipated as heat. See Supporting Information for movies.

Figure 4. Enhanced dehydration protection by a graphene coated contact lens. (a) Schematic of the experimental setup to measure the water evaporation rate througth contact lenses. **(b)** Weight loss measured with time on a hot plate at 38℃. **(c)** Water vapor transmission rate (WVTR) values of the contact lenses without and with graphene coating, derived from (b). The dehydration protection performance has been enhanced by ~30%.

Figure 5. Demonstration of a light emitting diode (LED) fabricated on a graphene-coated contact lens with electrode patterns. (a) A schematic view of the fabrication processes including the pattering of graphene by photolithography and O_2 plasma etching. **(b-c)** Optical and **(d)** SEM images of the patterned graphene on a conatact lens. **(e)** Raman specta of the patterned graphene on target substrates. **(f)** An assembled LED/graphene contact lens. **(g)** On/Off images of LED graphene lens operating voltage at 9 V**.**

Figure S1. Dehydration protection capbility of graphene-coated contact lenses with increasing graphene layers. (a) Weight loss of water in a container sealed with a contact lens. (**b**) WVTR values calcluated from the weight loss values in (a).

Figure S2. Test for estimating correlation factor between 4 point probe station and sheet resistance meter. (a) 4 point probe station and sheet

resistance meter (Dasol Eng., FPP-40K). (b) Reference graphene sample transferred on PET substrate. Graphene area is 2.5cm x 2.5cm. Ag paste was coated on graphene for electrodes. (c) V-I characteristics of each point. Resistance range of 196Ω ~ 243Ω (d) Data comparison of two measurement methods to estimate correlation factor. Finally, correlation factor 2.75 is obtained.

Figure S3. Schematic design and layer structure of smart contact lens with graphene contact lens. (a, b) Bottom Lens coated with graphene is positioned between eyeball and actual device circuit, cutting electromagnetic wave generated by actual circuit. Actual circuit assembly is attached on graphene lens using insulating adhesive.

Chapter 3

Figure 1. Schematic illustration of the mechanism of a graphene heater by EM waves. Graphene absorbs the energy of EM waves due to its strong diamagnetic response to EM, and dissipates the EM energy as heat energy, which can be utilized for fast and efficient heaters for various applications.

Figure 2. The graphene films transferred on target substrates. (a) An infrared scanning of the graphene heater transferred on quartz, while applying microwave during 10 s. The insets show an actual image of the graphene film. Scale bars, 1 cm. (b) The temperature variation of graphene heater transferred on target substrates. (c) Temperature profile comparison of Joule heating and EM heating at power 70W on 4 layers of graphene

films. (d) Saturation temperature uniformity of Joule heating and EM heating depending on number of graphene layers.

Figure 3. The heat distribution depending on charge mobility. (a) An infrared scanning of graphene heaters on SAMs irradiated by microwave during 10 s. Scale bar, 1 cm. (b) FET characteristics of graphene films depending on kinds of SAMs. (c) The temperature variation immediately measured after device fabrication. (d) The temperature variation measured after 7 d and annealing process.

Figure 4. Optical and IR photographs showing the EM-induced defogging of graphene coated vials. (a) The photograph before applying EM waves. Left is the graphene-coated bottle and right is the none-coated bottle. (b) The photograph after applying microwave during 5 s. (c) An infrared picture immediately obtained after microwave irradiation. Scale bars, 1 cm.

Figure 5. Raman spectra characteristics of the graphene heater by EM waves. (a) Variation of the G and 2D bands with irradiation time. (b) H2D/HG as functions of irradiation time. (c) A2D/AG as a function of the G peak shift. A2D and AG are the integral value of 2D peak and G peak respectively. (d) Position of the 2D peak as a function of the G peak shift (red line: p-doping effect, blue line: tensile/compressive stress following the arrow).

Figure S1. A schematic illustration on the fabrication processes of the graphene on a target substrate based on the use of pressure sensitive adhesive films (PSAFs).

Figure S2. Comparison on the heat-generation properties between dry-transferred and wet-transferred graphene films. (a) An actual photograph image of the graphene films transferred on a slide glass. (b,c) Infrared images showing the EM-heating of wet-transferred and dry-transferred graphene films after irradiating 70 W microwaves for 10 second, respectively.

Figure S3. Comparison between the EM heating of graphene on various substrates. (a, c and e) Infrared images of the graphene heaters transferred on Si3N4, PET, sapphire and SiO2/Si substrates, respectively. The inset images are the corresponding photograph images. Scale bars, 1 cm. (b, d and f) Temperature profiles corresponding to a, c and e, respectively.

Figure S4. (a) A schematic structure of the Joule-heating type graphene heater. (b, c) Temperature distribution of the Joule heater and the EM heater with 4-layer graphene films working at 70 W, respectively

Figure S5. (a) Optical and (b,c) IR photographs showing the Joule heating of monolayer graphene on a PET substrate.

Figure S6. Comparison of sheet reistance depending on the number of graphene layers and substrate types.

Chapter 1

General Introduction

1.1 Graphene

Graphene is two dimensional hexagonal single-layer sheet of sp2-hybridized carbon atoms. (as shown in Fig. 1) The theoretical background of graphene has been researched for 70 years,[1-2] and it was already predicted that the charge carriers of two dimensional graphene sheet would act like a massless Dirac fermion.

Since Novoselov and Geim of Manchester University successfully isolated single layer of graphite for the first time experimentally using a commercial Scotch tapes[3], graphene has attracted world-wide attentions and research interest because of its remarkable electrical, mechanical, chemical properties.

Some of the characteristics are the record high as shown in Fig. 2a.[5] The Intrinsic mobility of graphene at room temperature (RT) was estimated to be 200,000$cm^2v^{-1}s^{-1}$, higher than any other semiconductor. In spite of the remote interfacial phonon (RIP) scattering by the polar optical phonons of the SiO2 substrates, graphene on SiO2 revealed room temperature mobility of 40,000$cm^2v^{-1}s^{-1}$, comparable with the best InAs and InSb FETs. Graphene also has a remarkable thermal conductivity as shown in Fig. 2b.[6] Range between 3,000 and 5,000$Wm^{-1}K^{-1}$ of thermal conductivity around room temperature, which is absolutely above the bulk graphite limit, is measured in large-area suspended single layer graphene. As shown in Fig. 2c,[7] the outstanding mechanical property is also demonstrated. Young's modulus of single layer graphene was measured to be 1 TPa and intrinsic strength was measured to be 130 GPa, which corresponds to more than 200

times than that of steel. Single layer graphene has a high transmittance of ~97.7% as shown in Fig. 2d.[8]

Thanks to its outstanding electrical property, graphene can be utilized as very high performance electromagnetic (EM) wave shielding materials with extreme thin and transparent, light-weight. When an external magnetic field is given to graphene, high mobility of free electron in graphene makes orbital motion and induces oscillating magnetic moment to external electromagnetic field, showing diamagnetic property. In this way of magnetic field mirroring mechanism, graphene can be levitated on the strong permanent magnet field (static field), and can be also behaved as external EM wave (dynamic field) attenuating materials.[9-10] (Figure 3) It is reported that ideal graphene can block as much as 97.8% of EMI.[11] However, actual graphene synthesized experimentally has structural defects, and its EMI shielding effectiveness (SE) is reduced. (but still higher than other material). It is reported that the monolayer graphene synthesized by CVD has an average SE value of 2.27dB,[11] corresponding to 40% shielding, presenting 7 times (in terms of dB) greater SE than gold film. (as shown in Fig. 4 a,b)

Small gas molecules cannot pass through graphene, because its densely packed hexagonal lattice structure of carbon atoms. Moreover, mechanical flexibility and optical transmittance of graphene are expected to use flexible transparent barrier film.(Fig. 4. c,d)[12]

Owing to these unique and outstanding properties, graphene has drawn considerable attention for many applications such as electronic devices,

flexible display, energy devices, barrier films and membranes, heat spreader, battery electrodes, conductivity ink, bio-related applications, so on.[13]

Recently, contact lens platform devices,[14-17] which include electronics such as sensors, power module, antenna in itself, also have been developed for non-invasive and continuous analyzing glucose composition of tears as a substitute for blood glucose monitoring and for the diagnosis of glaucoma by measuring intraocular pressure. Lately, Google and Novartis released a prototype,[17](Fig. 6) named smart contact lens, with collaboration. Materials adopted to fabricate this contact lens platform devices should be light-weight for the convenience in wearing, and bio-compatible. I believe that graphene is the most suitable materials to realize such a wearable device. Graphene can be utilized as materials for electrode, barrier, EM shields of smart devices.

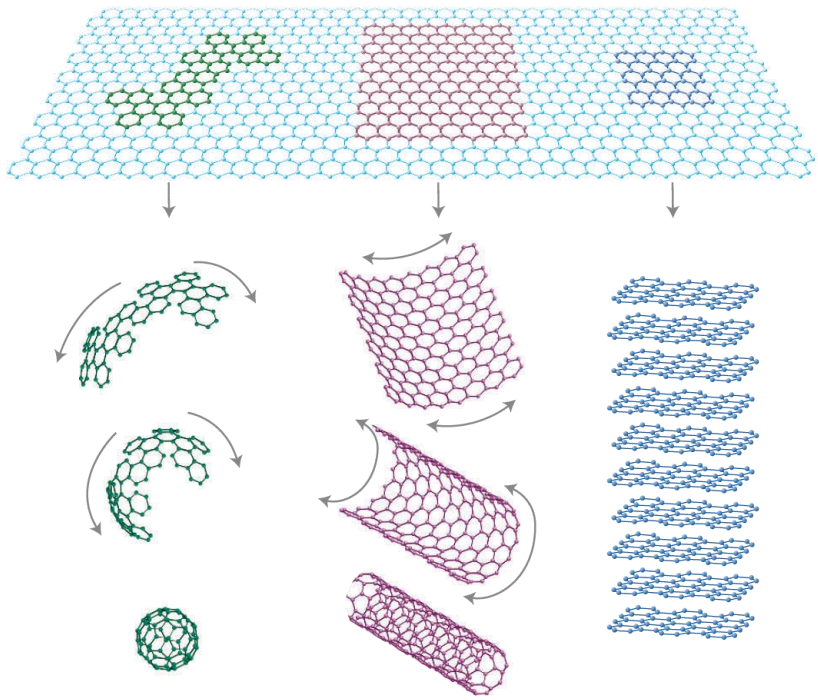

Figure 1. graphene is a 2D building materials of all other dimensionalities. It can be wrapped up into fullerene, rolled into carbon nanotubes or stacked into graphite. [Adapted from Ref. 4]

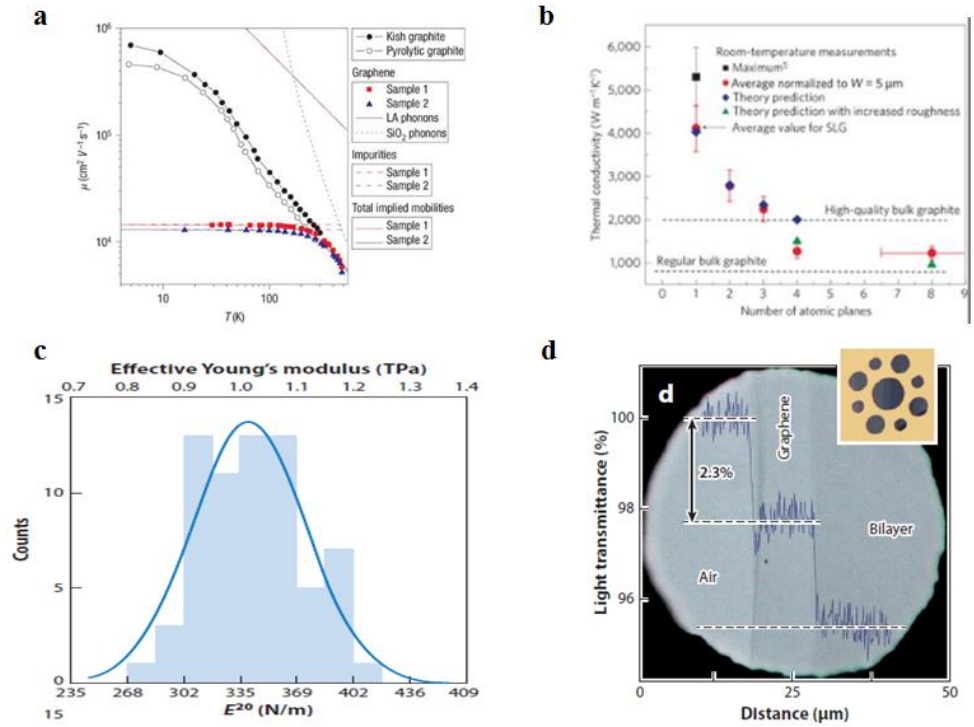

Figure 2. Outstanding Properties of Graphene (a) The temperature-dependant mobilities of graphene and graphite. [Adapted from Ref. 5] (b) Measured thermal conductibity as a function of the number of atomic planes in FLG. ted from Ref. 6] (c) Histogram of elastic stiffness of suspended graphene obtained from elastic response test results. ted from Ref. 7] (d) Photograph of a 50-nm aperture partially covered by graphene and its bilayer. ted from Ref. 8]

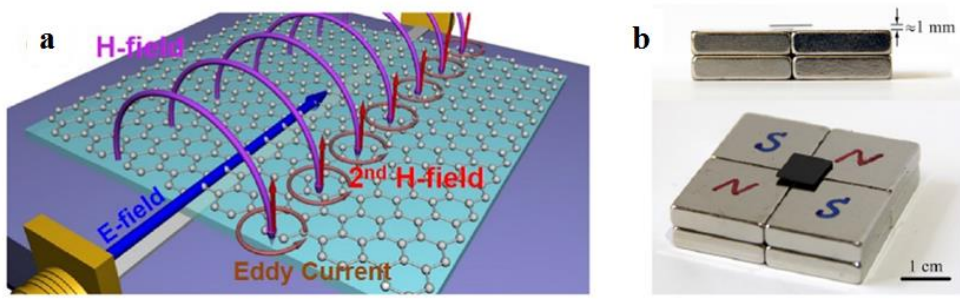

Figure 3. Diamagnetism of Graphene (a) Magnetic field illustration in the microstrip line overlaid with the graphene film [Adapted from Ref. 9] (b) A 10 × 10 × 0.3 mm3 piece of graphene sample produced from SiC is levitated by 1 mm above NdFeB magnets. [Adapted from Ref. 10]

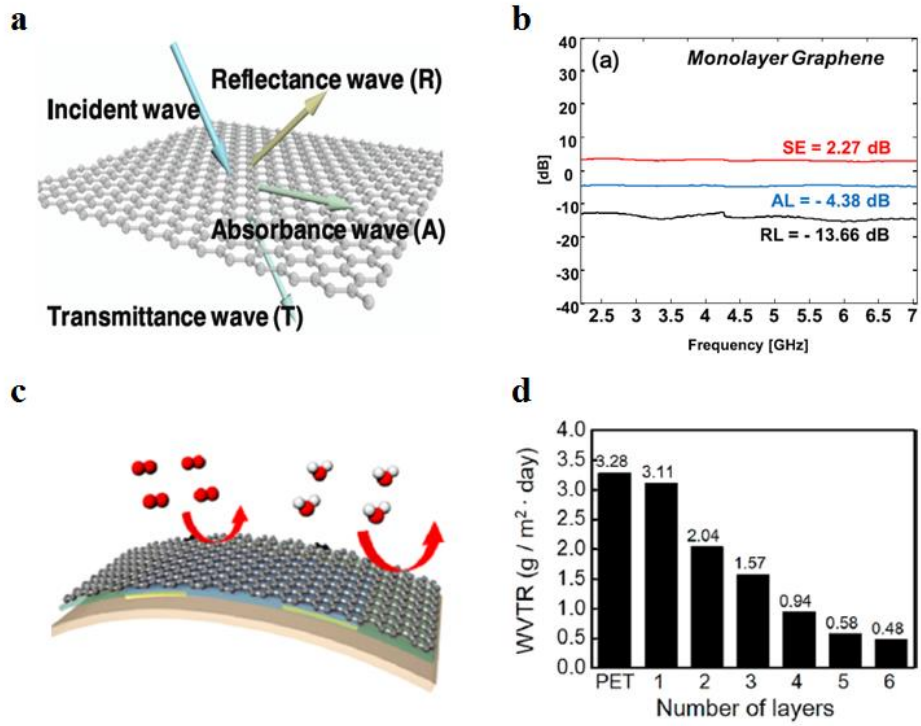

Figure 4. EMI Shielding and Gas Barrier Properties of Graphene (a) Description of wave dispersion on graphene. (b) The shielding effectiveness (SE), absorbance loss (AL), and reflectance loss (RL) of a monolayer graphene. [Adapted From Ref. 11] (c) Description of Gas Impermeability of graphene (d) WVTR values of graphene transferred on a PET film with respect to increasing number of graphene layers at 23 ^{o}C and 100% relative humidity. [Adapted From Ref. 12]

Figure 5. Overview of Applications of Graphene in different sectors ranging from conductive ink to chemical sensors, light emitting devices, composites, energy, touch panels and high frequency electronics. [Adapted from Ref. 13]

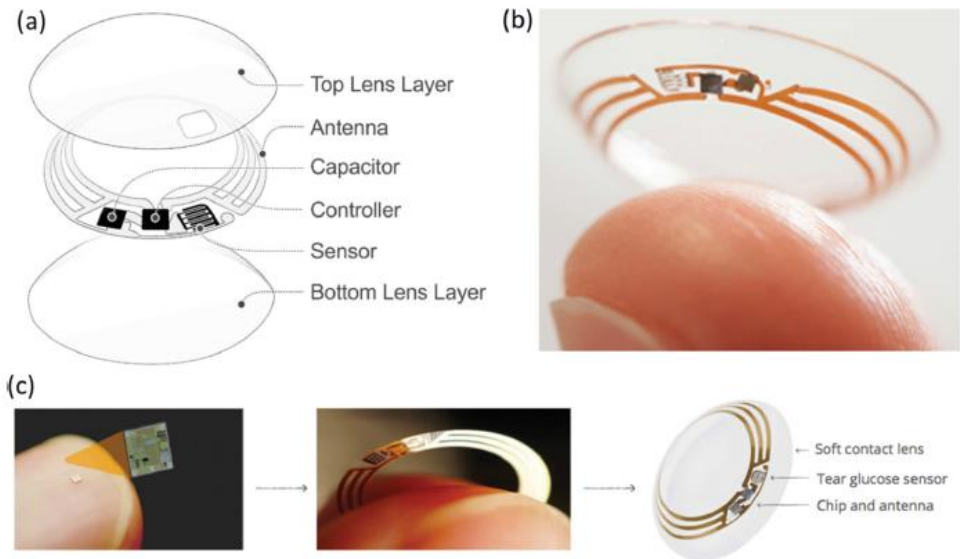

Figure 6. The contact lens sensor under co-development by Google and Novartis. It measures glucose concentration in tears using a miniaturized electrochemical sensor embedded into a hydrogel matrix. a) A schematic of the contact lens sensor, showing the electrical circuitry of the sensing system. b) The contact lens sensor prototype. c) The wireless chip, which is mounted, with the sensor, onto an electronic ring, and then embedded into the contact lens. [Adapted From 17] Copyright 2014, Google X.

1.2 Graphene Sysnthesis

First graphene synthesis was archived by mechanical exfoliation, called scotch tape method. Geim's group at Manchester University first succeeded in isolating single-layer graphene from graphite using commercial scotch tape in 2004.[18] Because 3D graphite consisted of many layers of 2D graphene by very weak interaction force between each layers, graphene layers can be peeled off onto the adhesive tape. A multiple peeling process leads to monolayer graphene. Figure 7. shows mechanical exfoliation of graphene and transferring on a target substrate.

Even though mechanical exfoliation method is simple, low cost method for obtaining very pure single domain graphene with nearly ideal properties, it has one large disadvantage. This method is limited by the size of the graphite flakes available (typically micrometer in size).

Furthermore, the thickness is difficult to accurately control, resulting in a lowyield problem, and so this is an unsuitable technique for mass production.

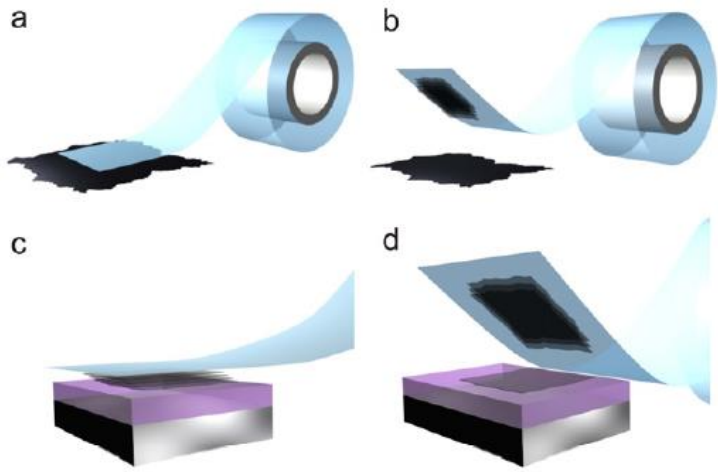

Figure 7. Micromechanical exfoliation of graphene. (a) Adhesive tape is pressed against a graphene. (b) Few layers of graphene are attached to the tape. (c) The tape with layers of graphene is pressed against a surface of target substrate. (d) Upon peeling off, the bottom layer is left on the substrate. [Adapted from Ref. 18]

Ruoff's group demonstrated a solution-based process for producing single layer graphene by chemical exfoliation. (as show in Fig. 8) Chemical exfoliation is an exfoliation method that uses strong acids and oxidants to obtain a flake of graphene oxide (GO).[19] The interaction forces between graphite layers become weak by oxidation of graphite using strong acids. The difference between hydrophilic oxidized graphene and hydrophobic graphite crystal allows water intercalate into graphene oxide and graphite crystal. During the dispertion process, oxidized graphene can be reduced with reductants. These reduced graphene oxides (rGO) can be deposited on various substrates.

This chemical oxfoliation method has a possibility of low cost synthesis and large scale production. However, the assembled graphene films show relatively poor electrical conductivity due to the poor interlayer junction contact resistance and structural defects formed during the vigorous exfoliation and reduction processes.

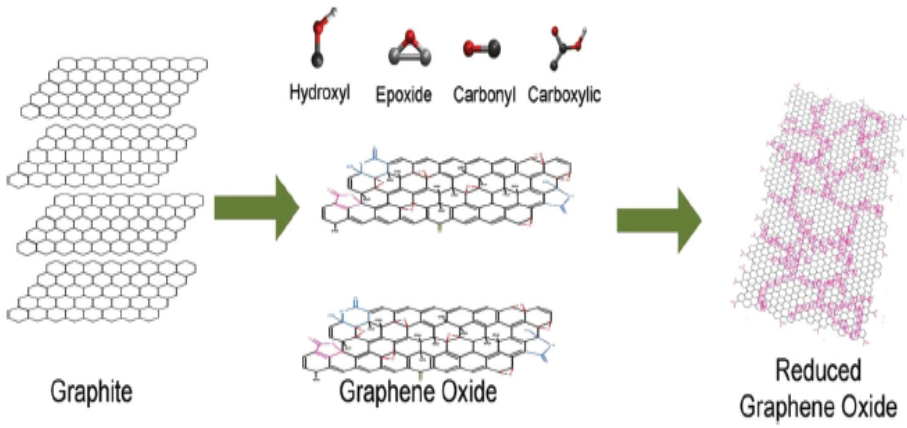

Figure 8. GO synthesis and reduction. Graphite can be oxidized with different procedures in the presence of strong acids. The GO flakes have the basal plane functionalized with epoxy and hydroxyl groups, both above and below it, and the edges with a variety of functional groups. This makes GO sheets defective. A partial restoration of the electronic properties is obtainable following different reduction strategies. [Adapted from Ref. 19]

The epitaxial growth of graphene on silicon carbide (SiC) in high vacuum and high temperature (1,000 ~ 1,600 ^{o}C) allows for the production of high quality and large area single layer and multilayer graphene.[20-21] Si is sublimated in this process, leaving carbon on the surface of SiC wafer. SiC wafers can be used as substrate for graphene based electronic devices. Graphene synthesized by this method has outstanding electrical properties, enabling it to be used in high-frequency (~100-GHz) electrical devices. However, SiC wafers are relatively expensive and limited in wafer production size. Transffering graphene grown in this way to arbitary substrates is also barrier for commercial adoption.

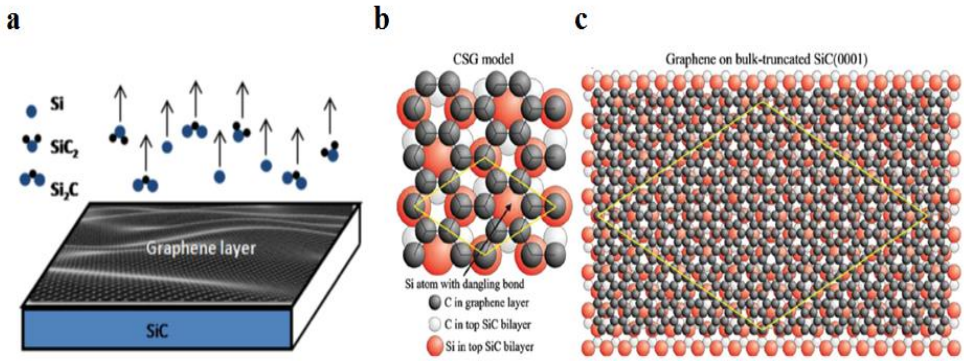

Figure 9. (a) Growth of epitaxial graphene on silicon carbide wafer via sublimation of silicon atoms [Adapted from Ref. 20]. (b) Top view of covalently bound stretched graphene (CSG) model on SiC(0001). (c) graphene on bulk-truncated SiC(0001) surface [Adapted from ref. 21]

Thermal Chemical Vapor Deposition (T-CVD) method is one of the most proper ways to produce high quality graphene without production size limitation. Graphene is grown on surface of transition metal catalyst, such as Cu,[22] Ni,[23] Ru,[24] or alloys, using CH2, C2H2 gas or solid sources [polystyrene, polyacrylonitrile, polymethyl methacrylate (PMMA) polymers] at near melting point of catalyst. Growth conditions such as the temperature dependence of carbon solubility in the metal and the gas flow rate and pressure determine the morphology (domain size and boundaries) and quality of graphene films grown by the T-CVD method. Among the transition metal catalyst, Cu is the most attractive for the synthesis of single layer graphene due to its low carbon solubility. Ni is often utilized for the synthesis of multi-layer graphene because of its high carbon solubility.

A metal catalyst is put into a CVD furnace and heated up to synthesis temperature (typically 1,000 ^{o}C) under H2 conditions. Then, carbon contained gas, such as CH4, flowed through furnace with H2. Finally, carbon atoms are deposited on surface of catalyst through chemical adsorption and makes continuous graphene.

Graphene grown on catalyst can be transferred to arbitrary substrate by wet transfer method. (As shown in Fig. 10) For this step, undesired cataylst and graphene should be removed. CVD graphene can be transferred using Thermal Release Tape (TRT) instead of PMMA. (Fig. 9)[26] TRT transfer method allows also continuous roll to roll production of graphene, which is more attractive for industrial purpose.[27]

Large scale graphene films synthesized by the CVD method shows tremendous potential of applications for transparent.

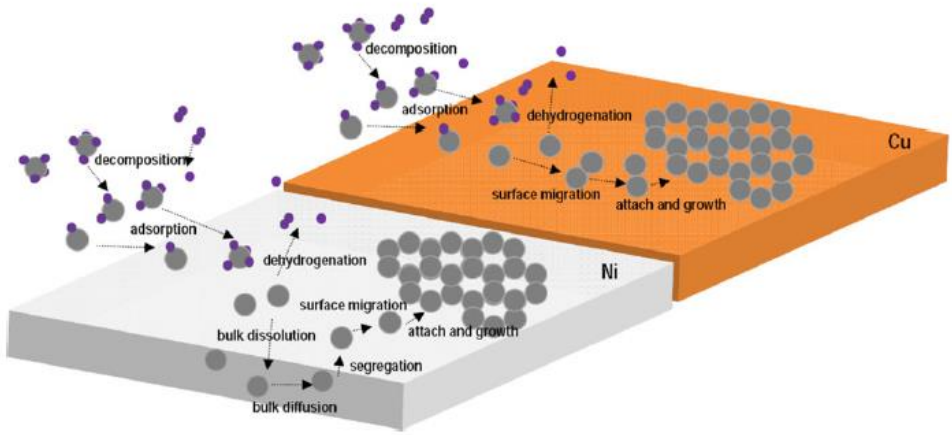

Figure 10. Growth kinetics in CVD-produced graphene on various catalysts: Case of CH4 on Ni and Cu. [Adapted from Ref. 22]

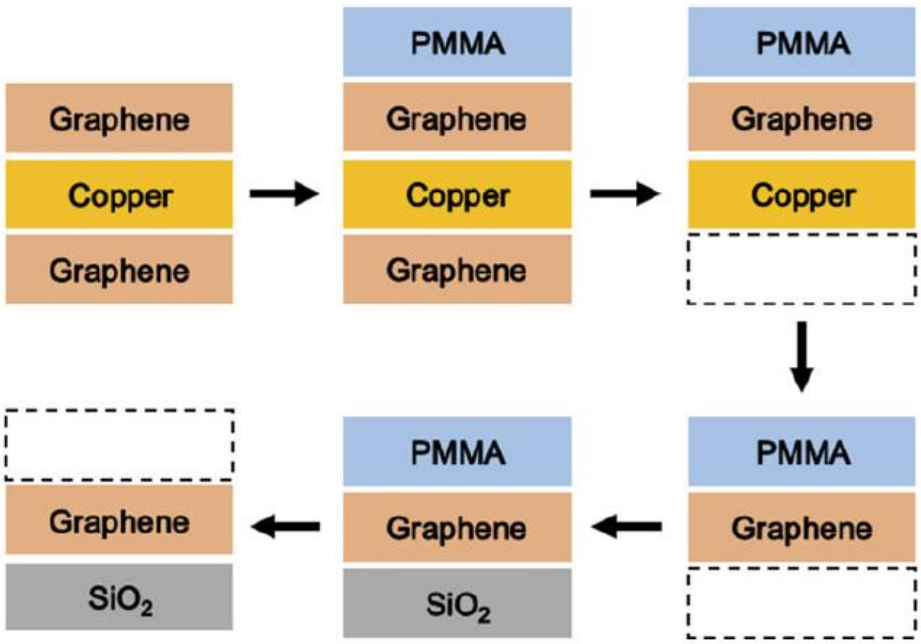

Figure 11. The process flow associated with the transfer of CVD-grown graphene onto SiO2. (i) one side of the graphene-covered copper foil is spin-coated with PMMA (950K A2), (ii) the PMMA is cured at 110 °C for 15 s on a hot plate, (iii) a diluted nitric acid solution (5 mL HNO3, 15 mL water) is used to etch away the graphene on the side of the copper foil that is not covered by PMMA, and (iv) a 1 M solution of ammonium persulfate is utilized at 70 °C to etch away the copper foil, leaving behind a strip of PMMA covered with CVDgrown graphene on one side. Subsequently, the PMMA strip is placed on a clean SiO2 wafer piece, and the PMMA is removed via dipping the sample into acetone. [Adapted from Ref. 26]

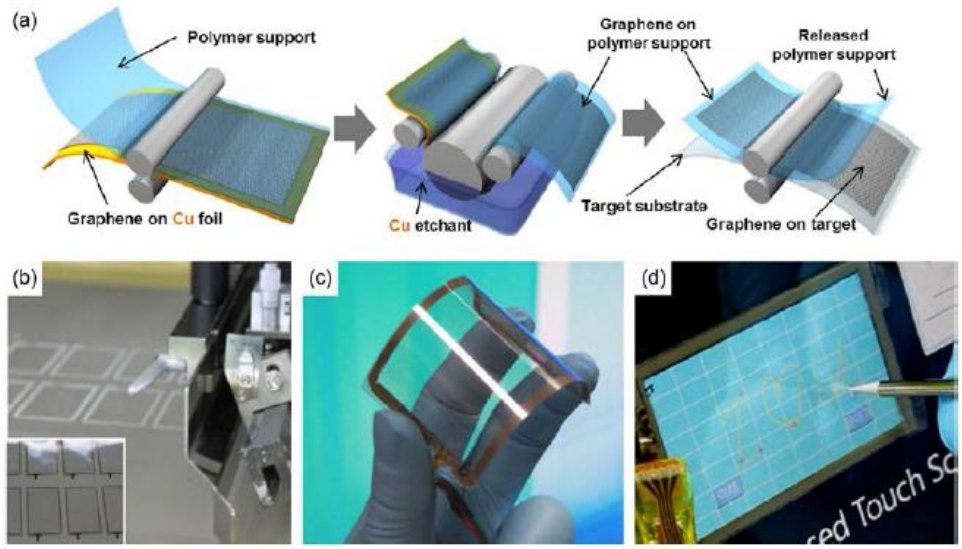

Figure 12. Roll to roll production of graphene and touch screen application. (a) Schematic of the roll-based production of graphene films grown on a copper foil. The process includes adhesion of polymer support such as thermal release tape, copper etching (rinsing) and dry-transfer-printing on a target substrate. (b-d) Photographs of application of graphene films grown by roll-to-roll method. (b) Screen printing process of silver paste electrodes on graphene/poly(ethylene terephthalate) (PET) films. The inset shows 3.1-inch graphene/PET panels patterned with silver electrodes before assembly. (c) An assembled graphene/PET touch panel showing outstanding _exibility. (d) A graphene-based touch-screen panel connected to a computer with control software. [Adapted from Ref. 27]

1.3 Scope of the Thesis

Graphene is an atomically thin carbon material with a two-dimensional hexagonal lattice that shows outstanding electrical and mechanical properties as well as excellent biocompatibility. Especially, EM attenuation and barrier property of graphene allow it to be used in fields of smart electronics. **In chapter2**, we report a CVD graphene-based highly conducting contact lens platform that reduces the exposure to EM waves and dehydration. Additionally, we demonstrate simple contact lens platform micro LED operating devices fabricated by CVD graphene-based conductive layers. Thus, we believe that the graphene-coated contact lens would provide a healthcare and bionic platform for wearable technologies in the future. **In chapter3**, we demonstrate EM wave shielding mechanism of graphene. Graphene generate a heat energy as a result of EM wave shielding. Therefore, this allows graphene heater to be used widely in fields of automobile defogging/deicing systems, smart heating windows and EM-wave detecting sensors.

1.4 References

1. Peierls R.; Quelques proprieties typiques des corpses solides. *Ann I H Poincare*, 5, 177 (**1935**).
2. Landau LD. Zur Theorie der phasenumwandlungen *II. Phys Z Sowjetunion*, 11, 26 (**1937**).
3. Novoselov, K. S.; Geim, A. K.; Morozov, S. V.; Jiang, D.; Zhang, Y.; Dubonos, S. V.; Grigorieva, I. V.; Firsov, A. A. Electric Field Effect in Atomically Thin Carbon Films. *Science* **2004**, 306, 666-669.
4. Geim, A. K.; Novoselov, K. S. The rise of graphene. *Nature Materials* **2007**, 6, 183.
5. Chen, J. H.; Jang, C.; Xiao, S.; Ishigami, M.; Fuhrer, M. S. Intrinsic and extrinsic performance limits of graphene devices on SiO2 Nature *Nanotechnol.* **2008**, 3(4), 206-209
6. Ghosh, S.; Bao, W.; Nika, D. L.; Subrina, S.; Pokatilov, E. P.; Lau C. N. and Balandin 1 A. A. Dimensional crossover of thermal transport in few-layer grapheme *Nature Materials.* **2010**, 9, 555-558
7. Lee, C.; Wei, X.; Kysar J. W. and Hone, J. Measurement of the Elastic Properties and Intrinsic Strength of Monolayer Graphene *Science* **2008**, 321, 385-388
8. Nair, R. R.; Blake, P.; Grigorenko, A. N.; Novoselov, K. S.; Booth, T. J.; Stauber, T.; Peres, N. M. R. and Geim, A. K. Fine Structure Constant Defines Visual Transparency of Graphene *Science* **2008**, 320, 1308-1308

9. Kang, J.; Kim, D.; Kim, Y.; Choi, J. B.; Hong, B. H.; kim, S. W. High-performance near-field electromagnetic wave attenuation in ultra-thin and transparent graphene films *2D Mater.* **2017**, 4, 025003

10. Li, Z.; Chen, L.; Meng, S.; Guo, L.; Huang, J.; Liu, Y.; Wang, W. and Chen X. Field and temperature dependence of intrinsic diamagnetism in graphene: Theory and experiment *PHYSICAL REVIEW B* **2015**, 91, 094429

11. Hong, S. K.; Kim, K. Y.; Kim, T. Y.; Kim, J. H.; Park, S. W.; Kim, J. H.; Cho, B. J. Electromagnetic Interference Shielding Effectiveness of Monolayer Graphene. *Nanotechnology* **2012**, 23, 455704.

12. Choi, K.; Nam, S.; Lee, Y.; Lee, M.; Jang, J.; Kim, S. J.; Jeong, Y. J.; Kim, H.; Bae, S.; Yoo, J.-B.; Cho, S. M.; Choi, J.-B.; Chung, H. K.; Ahn, J.-H.; Park, C. E.; Hong, B. H. Reduced Water Vapor Transmission Rate of Graphene Gas Ba rier Films for Flexible Organic Field-Effect Transistors. *ACS Nano* **2015**, 9, 5818−5824.

13. Ferrari, A. C.; Bonaccorso, F.; Falco, V.; Novoselov, K. S. Science and technology roadmap for graphene, related two-dimensional crystals, and hybrid systems *Nanoscale* **2015**, 7, 4598

14. Leonardi, M.; Pitchon, E. M.; Bertsch, A.; Renaud, P.; Mermoud, A. Wireless Contact Lens Sensor for Intraocular Pressure Monitoring: Assessment on Enucleated Pig Eyes. *Acta Ophthalmol.* **2009**, 87, 433−437.

15. Yao, H.; Shum, A. J.; Cowan, M.; Lahdesmaki, I.; Parviz, B. A. A Contact Lens with Embedded Sensor for Monitoring Tear Glucose Level. *Biosens. Bioelectron* **2011**, 26, 3290−3296.

16. Chen, G.-Z.; Chan, I.-S.; Lam, D. C. C. Capacitive Contact Lens Sensor for Continuous Non-Invasive Intraocular Pressure Monitoring. *Sens. Actuators A* **2013**, 203, 112−118.

17. Farandos, N. M.; Yetisen, A. K.; Monteiro, M. J.; Lowe, C. R.; Yun, S. H. Contact Lens Sensors in Ocular Diagnostics. *Adv. Healthcare Mater.* **2015**, 4, 792−810.

18. Novoselov, K. S. and Castro Neto, A. H. Two-dimensional crystals-based heterostructures: materials with tailored properties. *Physica. Scripta* **2012**, T146, 014006.

19. Bonaccorso, F.; Lombardo, A.; Hasan, T.; Sun, Z.; Colombo, L. and Ferrari, A. C. Production and processing of graphene and 2d crystals *Mater. Today* **2012**, 15, 564–589.

20. Mishra, N.; Boeckl, J.; Motta, N.; Lacopi, F. Graphene growth on silicon carbide: A review *Phys. Status Solidi A* **2016**, 213, 9, 2277-2289

21. Emtsev, K. V.; Speck, F.; Seyller, T. and Ley, L. Interaction, growth, and ordering of epitaxial graphene on SiC{0001} surfaces: A comparative photoelectron spectroscopy study *Phys. Rev. B* **2008**, 77, 155303.

22. Mattevi, C.; Kim, H.; Chhowalla, M. A. Review of chemical vapour deposition of graphene on copper. *J. Mater. Chem.* **2011**, 21, 3324.

23. Reina, A.; Jia, X.; Ho, J.; Nezich, D.; Son, H.; Bulovic, V.; Dresselhaus,

M. S. and Kong, J. Large area, few-layer graphene films on arbitrary substrates by chemical vapor deposition. *Nano Lett.* **2009**, 9, 30.

24. Sutter, P. W.; Flege, J. I.; and Sutter, E. A. Epitaxial graphene on ruthenium. *Nat. Mater.* **2008**, 7, 406.

25. Munoz, R.; Aleixandre, C. G. Review of CVD Synthesis of Graphene *Chem. Vap. Deposition* **2013**, 19, 297-322

26. Demirbas, T.; Baykara, M. Z. Nanoscale tribology of graphene grown by chemical vapor deposition and transferred onto silicon oxide substrates *J. Mater. Res.* **2016**, 31, 13

27. Bae, S.; Kim, H.; Lee, Y.; Xu, X.; Park, J. S.; Zheng, Y.; Balakrishnan, J.; Lei, T.; Kim, H. R.; Song, Y. I.; Kim, Y. J.; Kim, K. S.; Ozyilmaz, B.; Ahn, J. H.; Hong, B. H.; Iijima, S. Roll-to-roll production of 30-inch graphene films for transparent electrodes. *Nature Nanotechnol*. 5, 574 (2010. http://dx.doi.org/10.1038/nnano.2010.132.

Chapter 2

Smart Contact Lenses with Graphene Coating for Electro Magnetic Interference Shielding and Dehydration Protection

2.1 INTRODUCTION

Graphene, two dimensional hexagonal lattice structure of carbon atom, has been widely studied on various fields because of its remarkable electrical, mechanical, chemical properties since its first discovery by the mechanical exfoliation of graphite crystals.[1-5] Among its unique properties, outstanding electromagnetic wave absorption property and gas-impermeability have provided potentials to use graphene for electromagnetic interference (EMI) shielding and/or diffusion barriers.[6,7] It has been reported that graphene consists of only carbon atoms is much more effective, stable, light in weight EMI shielding materials than typical metal based materials, while the use of conventional EMI shielding materials based on metallic or magnetic materials has been limited by heavy weight and corrosion problems.[8-14] The recent advances in chemical vapor deposition (CVD) growth of large-area high-quality graphene is expected to enable the practical applications of graphene in our daily lives.[15-19, 24, 25]

Recently, with advances in electronics, micro/nanofabrication and information technology, wearable devices have been emerged and studied for the past few years. Contact lens type wearable devices also have been developed for various purposes including the diagnosis of glaucoma or diabetes by measuring intra ocular pressure or glucose composition of tears, where RF technologies using electromagnetic (EM) waves can be employed for power supply or signal.[20-23] However, in this case, there is a possibility of low temperature burn or dehydration, because the exposure to EM waves

is very continuous and close to eyes, even though electromagnetic wave interference (EMI) level generated from the device is considered relatively weak. Likewise, as a variety of wireless devices are connected to the internet of things (IoT) technologies, the exposure of our eyes to environmental EM waves will be steadily increasing. Thus, the EMI shielding function of the smart contact lenses is of great importance. In addition, it is known that wearing contact lenses for a long period of time possibly causes dry eye syndrome, which needs to be protected by keeping eye moisture as much as possible using a diffusion barrier. We believe that the CVD graphene is a suitable material for the EMI shielding and dehydration protection of contact lenses, because it has outstanding electrical properties as well as gas-impermeability along with high optical transmittance, mechanical flexibility, and environmental stability.

2.2 RESULTS AND DISCUSSION

Schematic working principle of the EMI shielding graphene contact lenses is shown in Figure 1a~d. Without graphene, the electromagnetic (EM) wave passes through the contact lens and directly absorbed by eyeballs, possibly causing a thermal damage potentially related to cataracts. In the case of using graphene, the EM wave is partially absorbed by the graphene layer on the contact lens, which reduces the EM energy delivered to the inner eyeballs (Figure 1a, b). When wearing contact lenses, tears play a role as lubricant, but the dehydration of the eyes may cause xerophthalmia (Figure 1c). The dehydration process can be prolonged by the graphene coating (Figure 1d).

Reliable graphene coating on the contact lens with a thin and soft hemispherical feature is a key for the experiment. For the conformal and durable coating of graphene on the lens, we used a template with same radius curvature of a contact lens. Overall fabrication processes are shown in Figure 1e. We synthesized the continuous monolayer graphene on a high purity Cu foil (99.99 %) using a typical chemical vapor deposition method with flowing 150 sccm methane and 15 sccm hydrogen gases at 1,000 ℃ in an 8-inch quartz tube, followed by coating with PMMA.[16] After etching away the Cu foil with 0.1 M ammonium persulfate ($(NH_2)_4S_2O_8$) aqueous solution and rinsing graphene in DI water, PMMA/Graphene was transferred on contact lens naturally attached on the template by surface tension of lens, steadily maintaining its feature during transfer process.

After baking for 30 minutes at 80 ℃ on a hot plate, the PMMA was removed by acetone. Here, the contact lens can be protected from acetone by the graphene layer on top. Finally, the graphene coating on the contact lens is completed by isolating the lens from the template using a sharp tip.

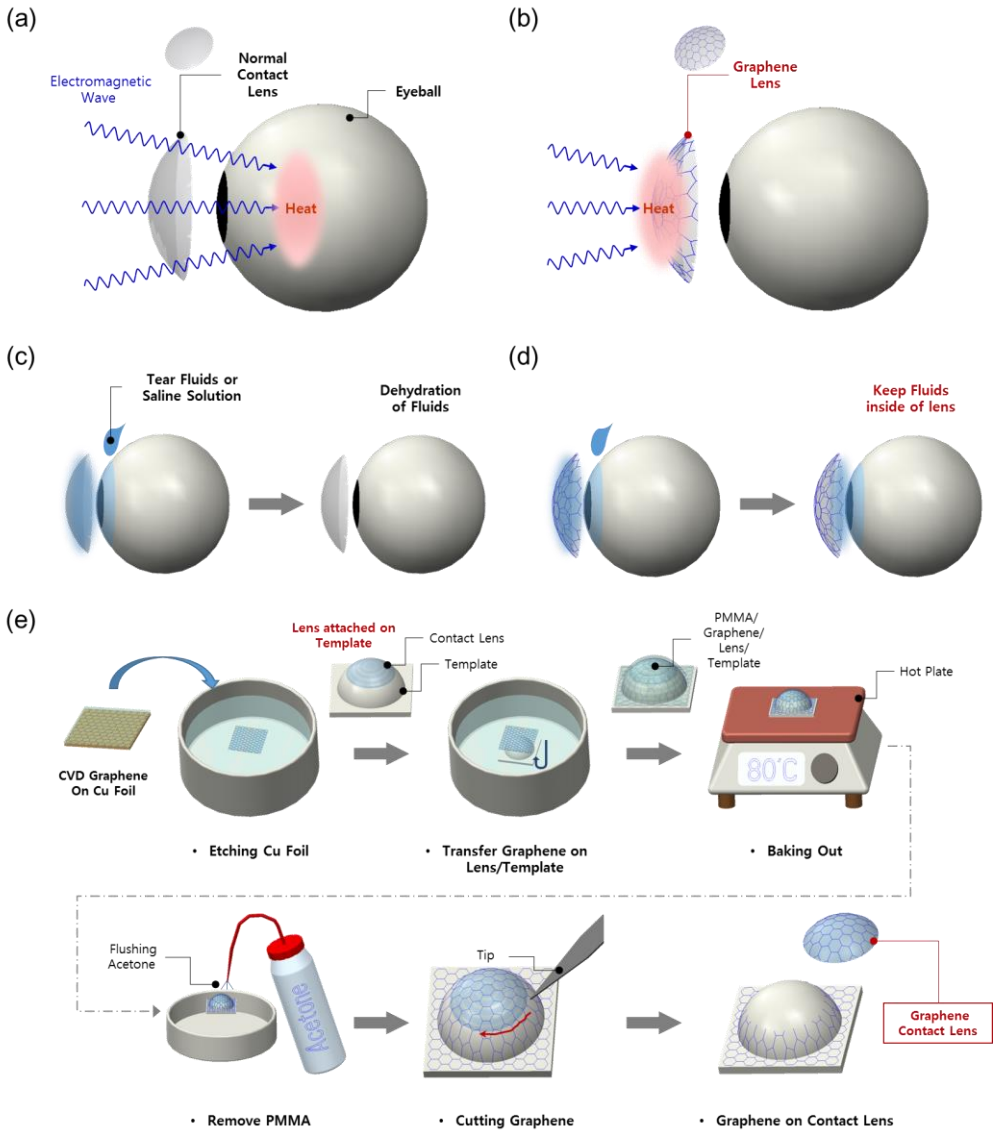

Figure 1. Schematic working principle of a graphene-coated contact lens and its fabrication process. (a) Electromagnetic (EM) wave passes through contact lens and absorbed by an eyeball, possibly causing heat damage inside. **(b)** EM energy is absorbed by graphene and disscipated as a heat before reaching the interior of the eye. **(c-d)** Dehydration of a contact lens can be reduced due to the gas-impermeability of graphene **(e)** The fabrication process of the graphene-coated contact lens.

Graphene lens was being crinkled up immediately after the process because it was exposed to air during the process, proceeding dehydration of lens. However, lens had been recovered its original feature by dipping in the saline solution for a while. A slight fall-off of transmittance, assumed 2.3 % at 550 nm, was found in graphene lens comparing with normal lens, but it was hard to recognize that difference (Figure 2c), suggesting that graphene lens could give us clear vision in wearing.[16] Electrical property of graphene lens has been investigated using 4 probe point measurement. PET sample coated with graphene (graphene PET) was also measured for the reference (Figure 2d). For the electrode, silver paste was formed on samples at intervals of 5 mm. To evaluate variation, 5 individual graphene lenses and 9 points in a graphene/PET sample were measured. Figure 2e is *I-V* plot of graphene lens with the resistance range of 199 Ω ~ 240 Ω, similar value with graphene PET. The sheet resistance of the graphene on the contact lens was calculated to be as low as 593 Ω/sq (± 9.3 %), as shown in Figure 2f.

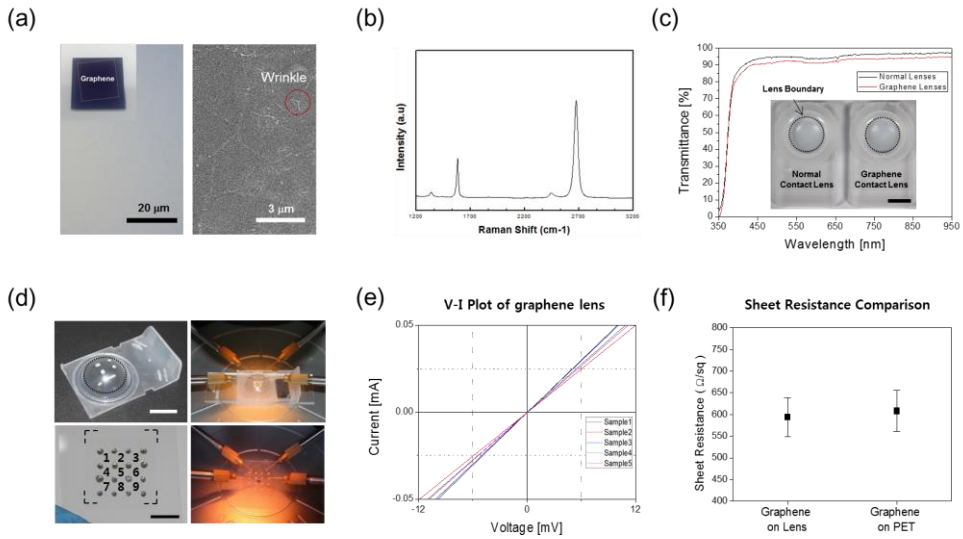

Figure 2. Optical and electrical properties of graphene films. **(a)** Optical and SEM images of graphene samples transferred on a SiO_2 substrate. **(b)** Raman spectrum of graphene showing monolayer thickness and low defect density. **(c)** Transmittance of a bare contact lens and a graphene-coated contact lens. Scale bar: 1cm. **(d-f)** Evaluation of electrical properties of graphene samples, including 4-point sheet resistance masurement and *I-V* characteristics.

To confirm the actual EMI-shielding effect of the graphene-coated contact lens, we irradiated a strong EM waves (120 W for 50 sec.) on to egg whites inside a microwave oven that has similar wavelength ranges with 4G LTE and Bluetooth (2.45 GHz) as shown in Figure 3. The results show that the thermal denaturalization, *i.e.* color change of the graphene-protected egg is considerably less than the case without graphene that protects EM waves.[10]

When the graphene is exposed to EM waves, the electrons in orbital motion induce oscillating magnetic moments in response to external magnetic field, which efficiently absorbs the EM energy and dissipates it as thermal energy. Therefore, the EM absorption efficiency can be evaluated by monitoring the heat generation from the graphene-coated contact lens. An IR camera was used to get thermal infrared images after applying EM radiation (120 W) on the samples inside a microwave oven for 20 seconds (Figure 3c). The results show that the temperature of the graphene-coated contact lens was rapidly increased above ~45 ℃, while the normal lens remained almost unchanged.

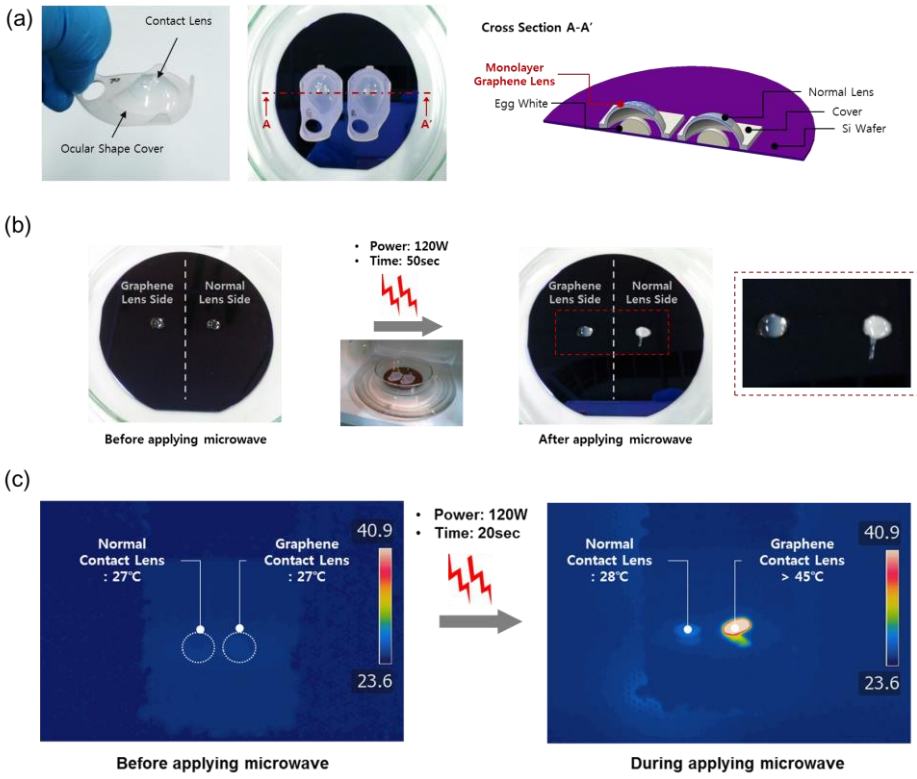

Figure 3. EMI shielding effect of the graphene-coated contact lens tested in a microwave oven. (a) Sample prapration for the microwave oven test. Egg whites on a Si wafer are covered with the contact lenses with and without graphene coating, respectively. **(b)** A microwave oven test showing the excellent EMI shielding effect of the graphene-coated contact lens. The egg white protected by graphene shows less thermal denaturalization. **(c)** IR camera images showing the the elevated temperature of the graphene-coated lens inside a microwave oven, indicating the EM energy is efficiently absorbed and dissipated as heat. See Supporting Information for movies.

To demonstrate the dehydration protection of graphene lens, we measured the water vaporization rate of water-filled vials capped with the contact lenses. The vial samples were placed on a hot plate at 38 ˚C, and the mass loss was measured on an electronic scale (Figure 4).[6] After 7 days, the weights of the normal and graphene-coated lenses were decreased by 0.8268 g and 0.5535 g, respectively (Figure 4c). The water vapor transmission rates (WVTRs) were estimated by considering the size of the lens, which has been reduced by 30 % (Figure 4d). We expect that the further improvement can be made by minimizing the defects on graphene during transfer and fabrication processes or by stacking multilayers of graphene.[7]

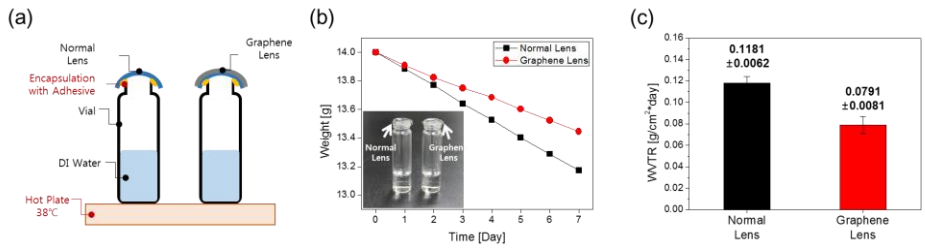

Figure 4. Enhanced dehydration protection by a graphene coated contact lens. (a) Schematic of the experimental setup to measure the water evaporation rate througth contact lenses. **(b)** Weight loss measured with time on a hot plate at 38℃. **(c)** Water vapor transmission rate (WVTR) values of the contact lenses without and with graphene coating, derived from (b). The dehydration protection performance has been enhanced by ~30%.

Finally, we demonstrated a simple micro-scale light emitting diode (LED) device fabricated on a contact lens with graphene electrodes. Figure 5a shows the fabrication processes of graphene electrodes by a conventional photolithography techniques.[24-25] The graphene was patterned on a SiO_2 substrate and transferred onto a contact lens by using PMMA as a supporting layer (Figure 5b, c). The negligible I(D)/I(G) ratio in Raman spectra indicate that no defect has been generated after patterning and transfer (Figure 5e). No meaningful change has been observed for high level EM exposure (~ 1 m from 100 W source) for more than 200 hrs. The pre-wired micro-LED was successfully working at ~ 9 V, implying that the graphene pattern on the contact lens is electrically continuous and robust enough to be used as an electrode (Figure 5g).

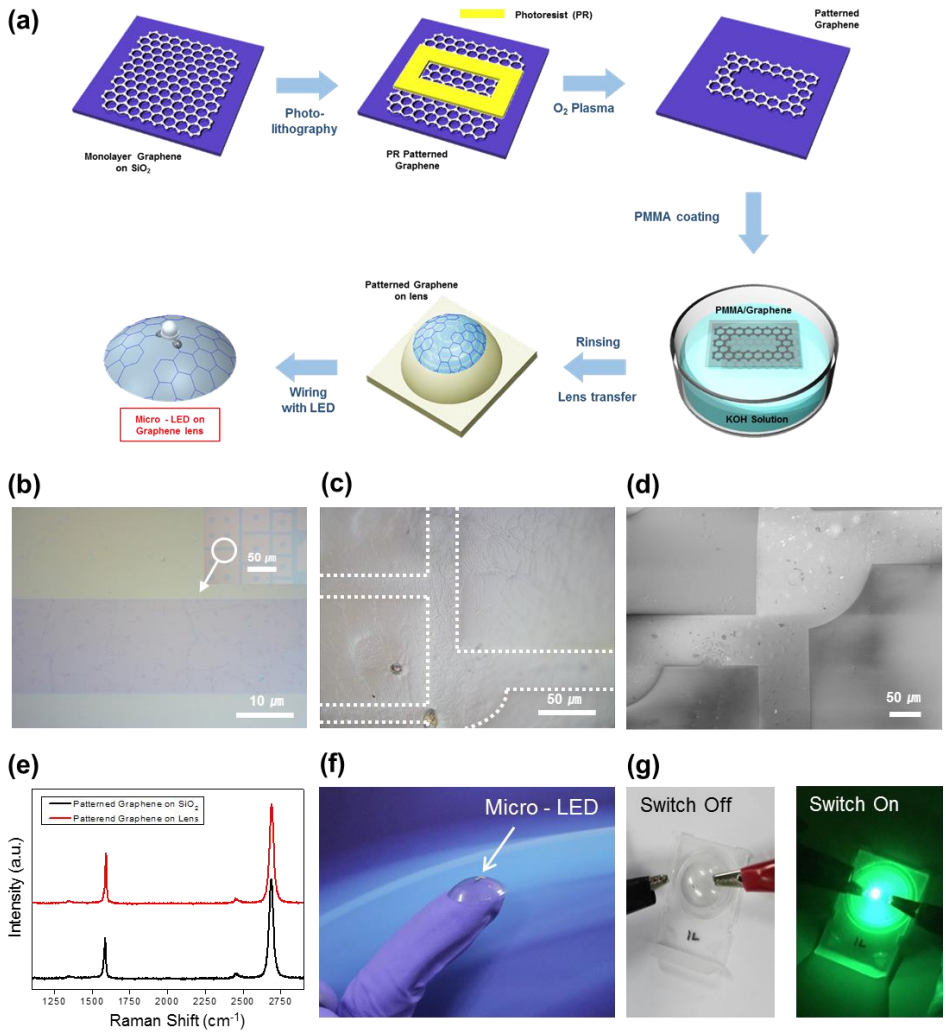

Figure 5. Demonstration of a light emitting diode (LED) fabricated on a graphene-coated contact lens with electrode patterns. (a) A schematic view of the fabrication processes including the pattering of graphene by photolithography and O_2 plasma etching. **(b-c)** Optical and **(d)** SEM images of the patterned graphene on a conatact lens. **(e)** Raman specta of the patterned graphene on target substrates. **(f)** An assembled LED/graphene contact lens. **(g)** On/Off images of LED graphene lens operating voltage at 9 V**.**

2.3 CONCLUSIONS

In conclusion, we demonstrated the conformal coating of a soft contact lens with CVD graphene and its application to EMI shielding and dehydration protection. The sheet resistance of ~593 Ω/sq. and the LED operation at 9 V indicate that the electrical properties of graphene can be maintained even after transfer and patterning. The EM wave shieling function of the graphene-coated contact lens was tested on egg whites exposed to strong EM waves inside a microwave oven. The results show that the EM energy absorbed by the graphene is released in the form of thermal radiation so that the damage on the egg whites can be minimized. We also demonstrated the enhanced dehydration protection effect of the graphene-coated lens by monitoring the change in water evaporation rate from the vial capped with the contact lens. Thus, we believe that the graphene-coated contact lens would provide a healthcare and bionic platform for wearable technologies in the future.

2.4 EXPERIMENTAL SECTION

Sample preparation. Monolayer graphene was synthesized on a high purity Cu foil (Alfa Aesar, 99.99%) utilizing 8 inch quartz tube CVD. The Cu foil was heated up to 1000 ℃ for 1 hour under a 15 sccm H_2 flow, and then 150 sccm CH_4 was inserted to grow graphene over 30 min at 1000℃. Then, the furnace was rapidly cooled down to room temperature under a 15 sccm H_2 flow. For the supporting and protecting of graphene, the PMMA solution was applied onto the graphene/Cu foil by a spin-coater. The Cu foil was etched away using 0.1 M ammonium persulfate ($(NH_2)_4S_2O_8$) over 5 hours. After rinsed with DI water, the floating graphene layer and the PMMA support film were transferred onto the target substrate (Si wafer, PET, contact lens). Si wafer with oxidation of 300nm and commercial contact lens (INTEROJO, 1Day Clalen) were used as substrate. To make encapsulation between contact lens and vial in water vapor transmittance rate test, we used 3M, Scotch AD6007 for the adhesive.

Fabrication of Graphene Lens with micro-LEDs. Single-layer graphene was transferred on a silicon wafer by PMMA-assisted wet-transfer. The micro-patterns of graphene (Width = 15 ㎛, Length = 50 ~ 200 ㎛) was generated by a typical photolithography process using a photoresist (AZ GXR-601, thickness = 1.5 ㎛). To transfer the micro-patterned graphene onto a contact lens, the PMMA supporting layer was coated on the patterned graphene again, and then, the silicon oxide layer was etched by 4 M potassium hydroxide (KOH) solution at 90 ℃. After rinsing with DI water, the floating graphene layers was transferred onto a contact lens by same method mentioned above. Finally, the pre-wired micro-LEDs (0402 SMD LED Green) was connected on the patterned graphene lens by silver paste.

Characterization. Optical microscopy was performed by Nikon ECLIPSE LV100ND, and the Raman spectra were recorded by a Raman spectrometer (RM 1000-Invia, Renishaw, 514nm). The sheet resistance was measured with 4-point probe nanovoltmeter (Keithley 6221) and DASOL FPP-40K. The current-voltage curve was measured by Agilent B2912A. We used a microwave oven of SAMSUNG Electronics (frequency = 2.45 GHz, Maximum output power = 700 W). An IR camera (FLIR T650sc) was used to monitor temperature change of samples. For the water vapor transmittance rate test, we used precision electronic scale with METTLER TOLEDO MS105DU. The SEM images were obtained by filed-emission scanning electron microscopy (FESEM, AURIGA Carl Zeiss).

Figure S1 represents weight loss of water-filled vials capped with the lens and graphene lenses depending on different graphene layers. After 3 days on a hot plate at 38℃, we fitted the measured weight as a function of the day and estimated the water vapor transmission rates (WVTRs) by considering the size of the lens. The increase in layer numbers leads to reduction of the water vapor transmission rates. The WVTRs of normal lens were 0.1666 ± 0.0009 g/cm^2*day. Increasing layer numbers of graphene on lenses, the WVTRs were decreased to 0.1523 ± 0.0013, 0.1015 ± 0.0018 and 0.0704 ± 0.0004 g/cm^2*day for the 1 layer-, 2 layer-, and 3 layer- graphene covered lens, respectively.

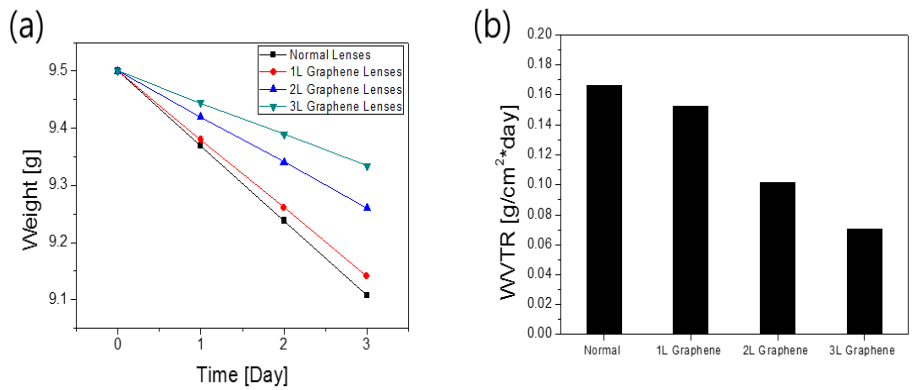

Figure S1. Dehydration protection capbility of graphene-coated contact lenses with increasing graphene layers. (a) Weight loss of water in a container sealed with a contact lens. (**b**) WVTR values calcluated from the weight loss values in (a).

(a)

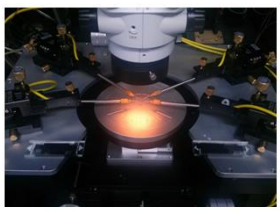

4 Point Probe Station

FPP-40K

(b)

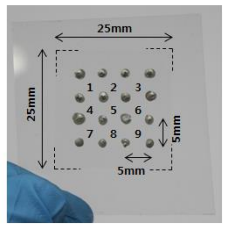

(c)

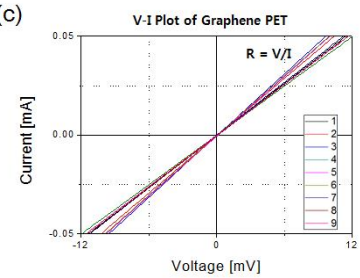

(d)

	FPP-40K	4 Point Probe Station	Estimated Correlation Factor
Position	Sheet Resistance [Ω/sq.]	Resistance [Ω]	
1	615.33	231.33	2.66
2	617.33	212.00	2.91
3	542.00	196.18	2.76
4	673.67	242.95	2.77
5	599.67	206.00	2.91
6	561.00	201.22	2.79
7	634.00	226.00	2.81
8	671.67	236.98	2.83
9	560.67	236.14	2.37
Average	**608.27**	**220.98**	**2.75**

Figure S2. Test for estimating correlation factor between 4 point probe station and sheet resistance meter. (a) 4 point probe station and sheet resistance meter (Dasol Eng., FPP-40K). (b) Reference graphene sample transferred on PET substrate. Graphene area is 2.5cm x 2.5cm. Ag paste was coated on graphene for electrodes. (c) V-I characteristics of each point. Resistance range of 196Ω ~ 243Ω (d) Data comparison of two measurement methods to estimate correlation factor. Finally, correlation factor 2.75 is obtained.

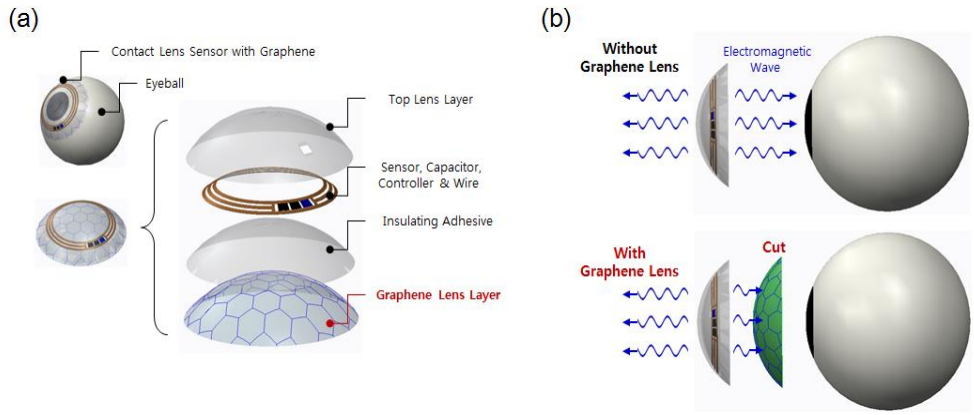

Figure S3. Schematic design and layer structure of smart contact lens with graphene contact lens. (a, b) Bottom Lens coated with graphene is positioned between eyeball and actual device circuit, cutting electromagnetic wave generated by actual circuit. Actual circuit assembly is attached on graphene lens using insulating adhesive.

The design of sensor part is the citation from [Ref.23] for the clear understanding of application concept.

2.5 REFERENCES

1. Novoselov, K. S.; Geim, A. K.; Morozov, S. V.; Jiang, D.; Zhang, Y.; Dubonos, S. V.; Grigorieva, I. V.; Firsov, A. A. Electric Field Effect in Atomically Thin Carbon Films. *Science* **2004**, 306, 666-669.
2. Geim, A. K.; Novoselov, K. S. The Rise of Graphene. *Nat. Mater.* **2007**, 6, 183-191.
3. Bolotin, K. I.; Sikes, K. J.; Jiang, Z.; Klima, M.; Fudenberg, G.; Hone, J.; Kim, P.; Stormer, H. L. Ultrahigh Electron Mobility in Suspended Graphene. *Solid State Commun.* **2008**, 146, 351-355.
4. Lee, C.; Wei, X.; Kysar, J. W.; Hone Measurement of the Elastic Properties and Intrinsic Strength of Monolayer Graphene. *Science* **2008**, 321, 385-388.
5. Bunch, J. S.; Verbridge, S. S.; Alden, J. S.; van der Zande, A. M.; Parpia, J. M.; Craighead, H. G.; McEuen, P. L. Impermeable Atomic Membranes from Graphene Sheets. *Nano Lett.* **2008**, 8, 2458-2462.
6. Nair, R. R.; Wu, H. A.; Jayaram, P. N.; Grigorieva, I. V.; Geim, A. K. Unimpeded Permeation of Water through Helium-Leak-Tight Graphene-Based Membranes. *Science* **2012**, 335, 442-444.
7. Choi, K.; Nam, S.; Lee, Y.; Lee, M.; Jang, J.; Kim, S. J.; Jeong, Y. J.; Kim, H.; Bae, S.; Yoo, J.-B.; Cho, S. M.; Choi, J.-B.; Chung, H. K.; Ahn, J.-H.; Park, C. E.; Hong, B. H. Reduced Water Vapor Transmission Rate of Graphene Gas Barrier Films for Flexible Organic Field-Effect Transistors.

ACS Nano **2015**, 9, 5818-5824.

8. Chung, D. D. L. Electromagnetic Interference Shielding Effectiveness of Carbon Materials. *Carbon* **2001**, 39, (2),279-285.

9. Chung, D. D. L. Materials for Electromagnetic Interference Shielding. *J. Mater. Eng. Perform.* **2000**, 9, 350-354.

10. Hong, S. K.; Kim, K. Y.; Kim, T. Y.; Kim, J. H.; Park, S. W.; Kim, J. H.; Cho, B. J. Electromagnetic Interference Shielding Effectiveness of Monolayer Graphene. *Nanotechnology* **2012**, 23, 455704.

11. Liang, J.; Wang, Y.; Huang, Y.; Ma, Y.; Liu, Z.; Cai, J.; Zhang, C.; Gao, H.; Chen, Y. Electromagnetic Interference Shielding of Graphene/Epoxy Composite. *Carbon* **2009**, 47, 922-925.

12. Chen, Z.; Xu, C.; Ma, C.; Ren, W.; Cheng, H. M. Lightweight and Flexible Graphene Foam Composites for High-Performance Electromagnetic Interference Shielding. *Adv. Mater.* **2013**, 25, 1296-1300.

13. Wang, C.; Han, X.; Xu, P.; Zhang, X.; Du, Y.; Hu, S.; Wang, J.; Wang, X. The Electromagnetic Property of Chemically Reduced Graphene Oxide and its Application as Microwave Absorbing Material. *Appl. Phys. Lett.* **2011**, 98, 072906.

14. Cao, M.-S.; Wang, X.-X.; Cao, W.-Q.; Yuan, J. Ultrathin Graphene: Electrical Properties and Highly Efficient Electromagnetic Interference Shielding. *J. Mater. Chem. C* **2015**, 3, 6589-6599.

15. Kim, K. S.; Zhao, Y.; Jang, H.; Lee, S. Y.; Kim, J. M.; Kim, K. S.; Ahn, J. H.; Kim, P.; Choi, J. Y.; Hong, B. H. Large-Scale Pattern Growth of

Graphene Films for Stretchable Transparent Electrodes. *Nature* **2009**, 457, 706-710.

16. Bae, S.; Kim, H.; Lee, Y.; Xu, X.; Park, J. S.; Zheng, Y.; Balakrishnan, J.; Lei, T.; Kim, H. R.; Song, Y. I.; Kim, Y. J.; Kim, K. S.; Ozyilmaz, B.; Ahn, J. H.; Hong, B. H.; Iijima, S. Roll-to-Roll Production of 30-inch Graphene Films for Transparent Electrodes. *Nat. Nanotechnol.* **2010**, 5, 574-578.
17. Bae, S.; Kim, S. J.; Shin, D.; Ahn, J.-H.; Hong, B. H. Towards Industrial Applications of Graphene Electrodes. *Physica Scripta* **2012**, T146, 014024.
18. Han, T.-H.; Lee, Y.; Choi, M.-R.; Woo, S.-H.; Bae, S.-H.; Hong, B. H.; Ahn, J.-H.; Lee, T.-W. Extremely Efficient Flexible Organic Light-Emitting Diodes with Modified Graphene Anode. *Nat. Photonics* **2012**, 6, 105-110.
19. Kang, J.; Kim, H.; Kim, K. S.; Lee, S. K.; Bae, S.; Ahn, J. H.; Kim, Y. J.; Choi, J. B.; Hong, B. H. High-Performance Graphene-Based Transparent Flexible Heaters. *Nano Lett.* **2011**, 11, 5154-5158.
20. Leonardi, M.; Pitchon, E. M.; Bertsch, A.; Renaud, P.; Mermoud, A. Wireless Contact Lens Sensor for Intraocular Pressure Monitoring: Assessment on Enucleated Pig Eyes. *Acta Ophthalmol.* **2009**, 87, 433-437.
21. Yao, H.; Shum, A. J.; Cowan, M.; Lahdesmaki, I.; Parviz, B. A. A Contact Lens with Embedded Sensor for Monitoring Tear Glucose Level.

Biosens. Bioelectron. **2011**, 26, 3290-3296.

22. Chen, G.-Z.; Chan, I.-S.; Lam, D. C. C. Capacitive Contact Lens Sensor for Continuous Non-Invasive Intraocular Pressure Monitoring. *Sens. Actuators A: Phys.* **2013**, 203, 112-118.

23. Farandos, N. M.; Yetisen, A. K.; Monteiro, M. J.; Lowe, C. R.; Yun, S. H. Contact Lens Sensors in Ocular Diagnostics. *Adv. Healthc. Mater.* **2015**, 4, 792-810.

24. Park, J. U.; Nam, S. W.; Lee, M. S.; Lieber, C. M. Synthesis of Monolithic Graphene–Graphite Integrated Electronics. *Nat. Mater.* **2012**, 11, 120-125.

25. Lee, M. S.; Lee, K.; Kim, S. Y.; Lee, H.; Park, J.; Choi, K. H.; Kim, H. K.; Kim, D. G.; Lee, D. Y.; Nam, S. W., Park, J. U. High-Performance, Transparent, and Stretchable Electrodes Using Graphene-Metal Nanowire Hybrid Structures. *Nano Lett.* **2013**, 13, 2814-2821.

Chapter 3

Efficient heat generation in large-area graphene films by electromagnetic wave absorption

3.1 INTRODUCTION

Graphene has intrigued the interest of worldwide researchers due to its extraordinary electrical[1-4], mechanical[5,6], optical[7,8], and chemical[9-11] properties for various application[12-19]. In particular, the superior thermal conductivity of graphene lead many researchers into using graphene as core materials in heating applications[20,21]. Through the development of chemical vapor deposition (CVD)[22] and roll-to-roll process for large size graphene film synthesis[23], graphene received much attention as a flexible and transparent material in heater application[24] and even considered as an alternative to indium tin oxide (ITO)-based heaters[25,26]. The general heat generation mechanism of carbon materials is known to be Joule heating[20,27]. Joule heating is the process by which the movement of current through a conductor releases heat due to its resistance. However, the heating rate and efficiency of the graphene-based heater arising from Joule heating was limited by the conductivity of graphene which is related to the restraint of sheet resistance[28,29].

Here we report a novel method to generate heat on a large-area graphene film by applying the unique electromagnetic (EM) wave absorption property[30] of graphene materials. The EM wave induces an oscillating magnetic moment generated by the orbital motion of moving electrons in graphene, which efficiently absorbs the EM energy and dissipates it as a thermal energy (figure 1). In this case, we can expect that the electron mobility is important than the conductivity of graphene,

because the diamagnetic moment is directly proportional to the speed of electron in an orbital motion. Thus, we tried to control the carrier concentration of graphene by functionalizing substrates with self-assembled monolayers (SAM), and found that the graphene film that shows the Dirac voltage close to zero can be more efficiently heated by EM waves. In addition, the temperature gradient also depends on the number of graphene layers due to the increased accumulation of diamagnetism. This heating method would be advantageous for sensing of EM waves, defogging smart windows, highly efficient and quick heating, etc.

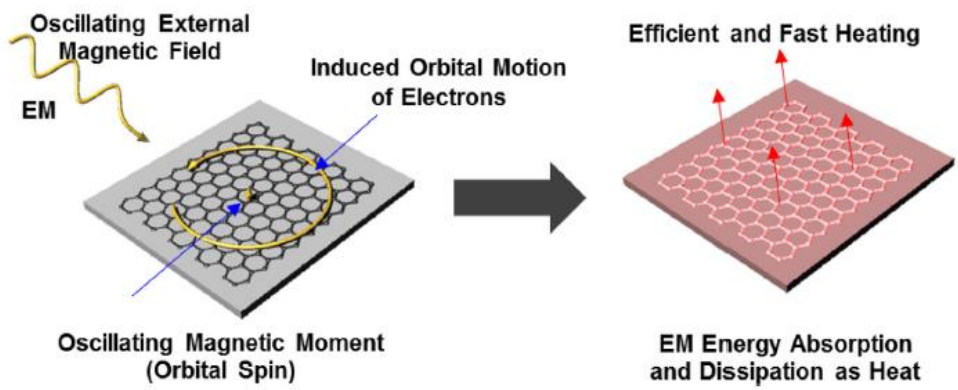

Figure 1. Schematic illustration of the mechanism of a graphene heater by EM waves. Graphene absorbs the energy of EM waves due to its strong diamagnetic response to EM, and dissipates the EM energy as heat energy, which can be utilized for fast and efficient heaters for various applications.

3.2 RESULTS AND DISCUSSION

First, a large scale graphene film was synthesized by CVD on a high purity Cu foil and dry transferred to a target substrate. The conventional wet transfer method produces unnecessary dipoles between graphene and substrates by the interference of water droplets causing increase in heat generation. In addition, unwanted doping effects on graphene film are produced by metal etching solution and polymer residues[31]. Recently dry transfer using pressure sensitive adhesive films (PSAF) instead of wet transfer using a supporting polymer was developed to avoid these problems [32]. Therefore, in order to accurately analyze the heating mechanism of graphene by EM waves, the dry transfer method is inevitable (figures S1 and S2 ((stacks.iop.org/TDM/4/025037/mmedia))).

Figures 2(a) and (b) shows infrared (IR) scanning of graphene surface on quartz substrates irradiated by EM wave at 2.45 GHz. The reason why we chose microwave spectra in these experiments is due to the frequent use of microwave in our everyday life. Unlike natural quartz, graphene film coated quartz plate generates heat depending on the number of stacked layers. The reason that the heat generation increases with number of graphene layers is due to not only Joule heating between the graphene layers but also the accumulated diamagnetism proportional to the increment of layers. Except quartz, various substrates coated by graphene films show heat gradient by EM waves (figure S3). Figure 2(c) represents the comparison of time consumed for Joule heating and EM heating to reach the saturation

temperature. The typical Joule heating occurs from electron scattering on defect sites of graphene film. So the heat is generated initially at the defect site and diffuses to the entire film as form of additional electron scattering and lattice vibration[24]. Therefore, Joule heating process requires adequate amount of time. In case of EM heating the entire graphene film absorbs EM wave, therefore, it shows faster increase in temperature compared to the Joule heating. This difference also affects the temperature uniformity after the saturation temperature. The power control of EM heating and joule heating will be further elaborated on method section. Figure 2(d), for Joule heating in monolayer graphene, indicates the local generation of heat due to the difficulty in achieving uniform sheet resistance. But as graphene films are stacked in layers their sheet resistance becomes more uniform, and uniform temperature distribution can be observed at four layer stacked graphene. Whereas in EM heating, the entire surface of film absorbs EM wave as mentioned above, so even in monolayer graphene uniform temperature distribution is detected. The uniformity of saturation temperature also increases proportionally to the stacked layers of graphene films in EM heating. This phenomena in EM heating is related to the Joule heating occurring at mismatch lattices between layers and also due to the increase in EM absorption following multiple stacked graphene layers[33]. Detailed comparison experiment with Joule heating is described in supporting information figure S4.

To understand the mechanism of the heat generation by the absorption of EM waves, we describe experimental results obtained from changing the

temperature of the graphene film on the Si3N4 substrates under the different Dirac-voltage and charge carrier mobility. The ordered close-packed structure of SAMs can suppress the substrate-induced doping on graphene, thereby the Dirac-voltage and work-function of the graphene could be tuned by SAMs[34,35]. Thus, we functionalized the substrates with SAMs to control the Dirac-voltage and mobility.

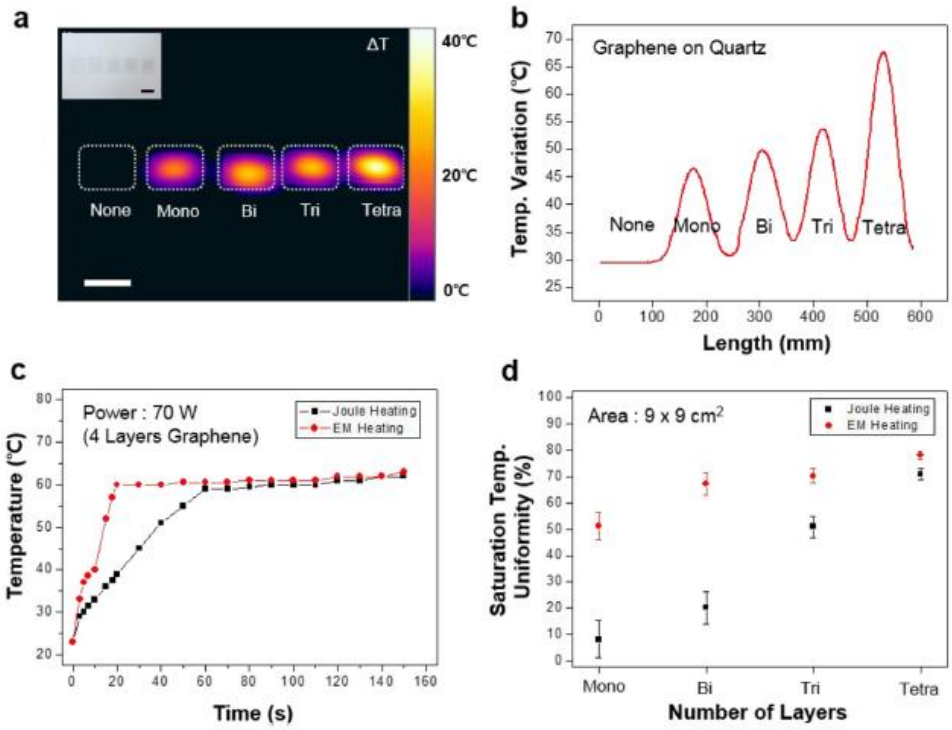

Figure 2. The graphene films transferred on target substrates. (a) An infrared scanning of the graphene heater transferred on quartz, while applying microwave during 10 s. The insets show an actual image of the graphene film. Scale bars, 1 cm. (b) The temperature variation of graphene heater transferred on target substrates. (c) Temperature profile comparison of Joule heating and EM heating at power 70W on 4 layers of graphene films. (d) Saturation temperature uniformity of Joule heating and EM heating depending on number of graphene layers.

Figures 3(a) and (b) demonstrate that the graphene which shows the Dirac-voltage close to zero can be more efficiently heated by EM waves. Two types of silanes move the Dirac-voltage of pristine graphene close to zero, and the γ-aminopropyltriethoxysilane (APS) brought the gradient closer to zero than that of octadecyltrichlorosilane (OTS). As Dirac-voltage approached to zero, graphene devices showed increasing electron mobility of 633 ± 108 (pristine), 1123 ± 232 (OTS), and 1568 ± 461 (APS) cm2 V−1 s−1 respectively. The differences of heat generation has such tendency, the diamagnetic properties were directly proportional to the electron mobility in graphene film. The relative permittivities remain the same, because the comparatively long chains of the two silanes produce very weak dipole and the SAMs functions to subtly reduce the effect of substrates. Therefore, the heat distribution of graphene films immediately measured after device fabrication in figure 3(c) was originated from differences of mobility. Interpreting the following phenomena with the conventional Joule heating mechanism, the temperature in samples functionalized with OTS SAMs should increase higher as they show better conductivity in FET measurement compared to those functionalized with APS SAMs. However, in this experiment APS SAMs functionalized samples showed superior heat generation and this can be explained with the increased diamagnetism due to electron mobility in EM heating. The adsorption of impurities is inevitable during the fabrication processes, and

some molecules with dipole moments may cause additional thermal activation by EM waves, possibly affecting the heating efficiency. To exclude it, we employed the post annealing process that minimizes the surface impurities, and confirmed that the influence of impurities on the heating efficiency is negligible. Therefore, we performed annealing process in Ar/He circumstance at 300 °C after 7 d to remove these additional dipole factors and confirmed that the heat distribution originated from the relative mobility differences (figure 3(d)).

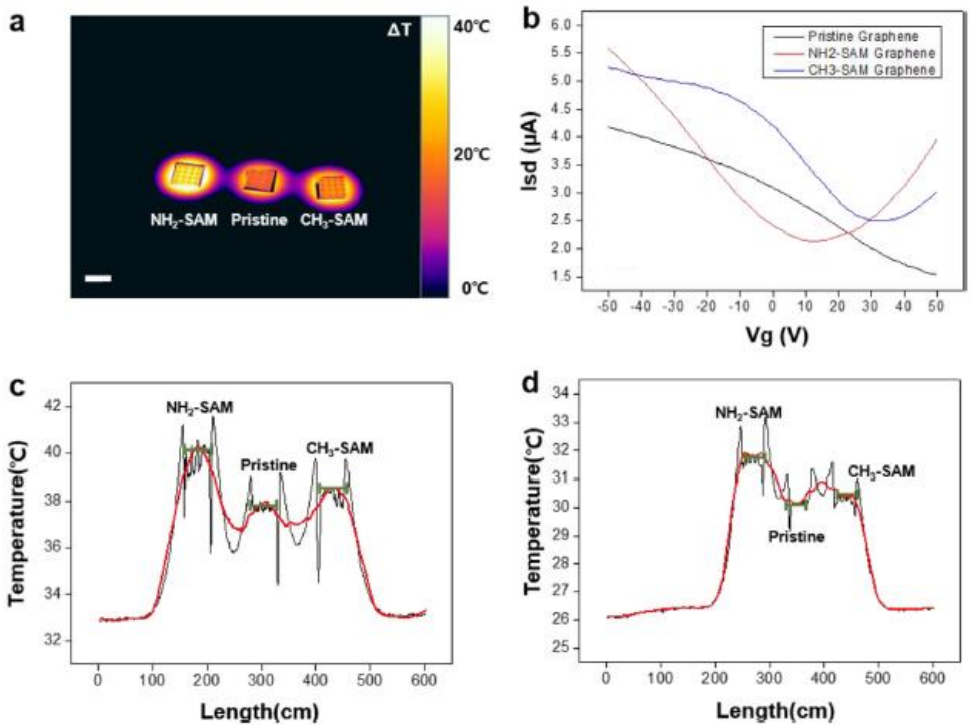

Figure 3. The heat distribution depending on charge mobility. (a) An infrared scanning of graphene heaters on SAMs irradiated by microwave during 10 s. Scale bar, 1 cm. (b) FET characteristics of graphene films depending on kinds of SAMs. (c) The temperature variation immediately measured after device fabrication. (d) The temperature variation measured after 7 d and annealing process.

Figure 4(a) shows the contrast of frost and steam on the non-coated glass bottle and the graphene-coated glass bottle. The graphene films can be applied to curved surface by dry transfer and EM waves even without electrodes to generate the Joule-heating. Irradiated by microwave for 5 s, the graphene-coated glass bottle was completely clear compared to the non-coated glass bottle (figures 4(b) and (c), movie S1). This result shows apparent contrast with regular Joule heating which requires at least 30 s to reach the intended saturation gradient. Also heating on curved surface via Joule heating is difficult as additional electrodes are needed (figure S5). This suggests that the graphene heater by EM waves is applicable to smart windows and EM wave detectors.

Figure 4. Optical and IR photographs showing the EM-induced defogging of graphene coated vials. (a) The photograph before applying EM waves. Left is the graphene-coated bottle and right is the none-coated bottle. (b) The photograph after applying microwave during 5 s. (c) An infrared picture immediately obtained after microwave irradiation. Scale bars, 1 cm.

The EM waves can give P-doping effect to graphene films[36] and may reduce the efficiency as a practical heater. Figure 5(a) shows the variation of Raman spectrum during the time of irradiated EM wave in graphene films. P-doping effects were confirmed via the ratio of intensity and area of G peak and 2D peak (figures 5(b) and (c)). Convincingly in figure 5(d), analyzing the 2D peak shift following the G peak shift, the graphene film exposed to EM wave showed P-doping effects to some degree. However as indicated previously, less than 1 min is need to reach the desired saturation temperature, thus practical P-doping followed by EM wave is not obtainable due to time limitation. Thus, the quick heat generation and stability of graphene films by EM waves can be applied to produce transparent and flexible heaters.

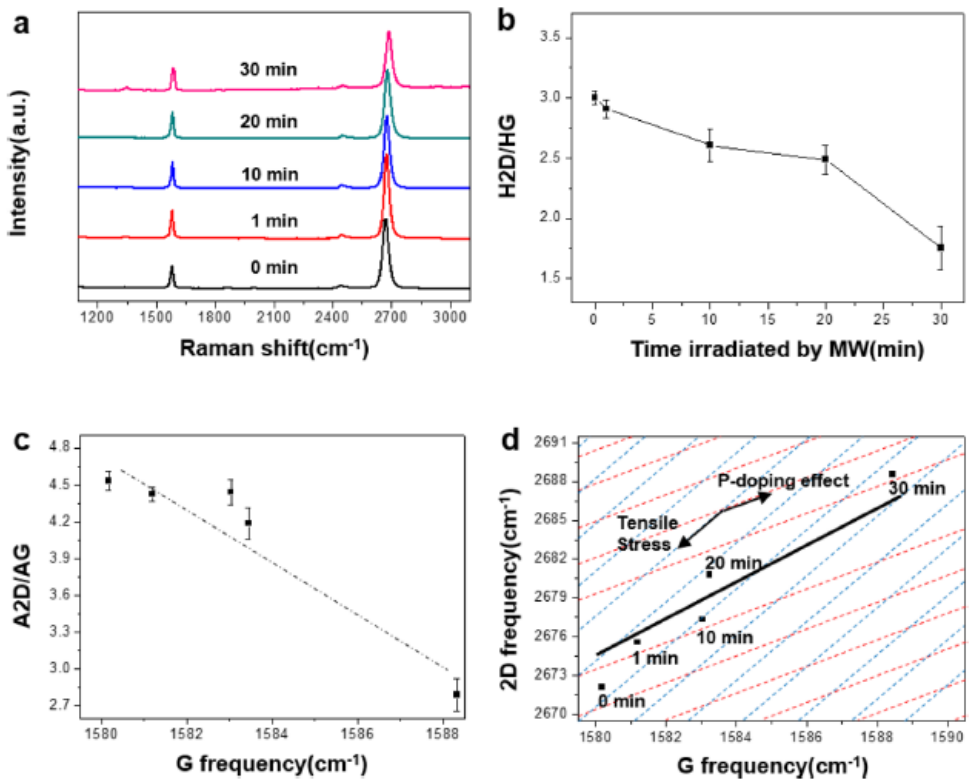

Figure 5. Raman spectra characteristics of the graphene heater by EM waves. (a) Variation of the G and 2D bands with irradiation time. (b) H2D/HG as functions of irradiation time. (c) A2D/AG as a function of the G peak shift. A2D and AG are the integral value of 2D peak and G peak respectively. (d) Position of the 2D peak as a function of the G peak shift (red line: p-doping effect, blue line: tensile/compressive stress following the arrow).

3.3 CONCLUSIONS

In conclusion, we have successfully demonstrated a graphene-based heater which can be triggered by EM waves and proved the mechanism of heat generation. We found that EM wave absorption phenomena is related to the diamagnetic properties of the graphene, which was confirmed by the heating efficiency that is inversely proportional to the electron mobility of graphene. The temperature response and heat distribution results show that the performance of EM waves-based heater is superior to that of the conventional Joule heating-based heaters. In particular, the EM-based graphene heaters can be easily fabricated without the additional equipment such as electrode and electric wires. Therefore, this allows graphene heater to be used widely in fields of automobile defogging/deicing systems, smart heating windows and EM-wave detecting sensors.

3.4 EXPERIMENTAL SECTION

Graphene synthesis and transfer

Graphene film was synthesized by CVD. Monolayer graphene was produced on a 25 μ m thick Cu foil (Alfa Aesar, 99.999%) with 70 mTorr H2 (4 sccm) and 650 mTorr CH4 (35 sccm) gas flow rate at 1000℃. The synthesized graphene on Cu was coated by PSAF and followed by Cu catalyst etching using 0.1 M ammoniumpersurfate (APS) solution. The graphene films on the PSAF was rinsed with distilled water and conserved in dehydrated condition for dry transfer. The graphene on the PSAF was affixed to the target substrates by weak pressing or roll to roll process. The comparison of multilayer graphene heaters can be fabricated by conventional wet transfer method and repeatedly transferring these graphene onto the same substrate.

EM heating and joule heating comparison

We used a microwave oven manufactured by SAMSUNG electronics, as the source of microwaves (frequency = 2.45 GHz). The power of EM heating can be manipulated from 50 W to 700 W with this equipment. We calculated the joule heating power depending on the number of graphene layers using the following equations as shown figure S6;

$$P = VI = V2/R$$

$$R = \_(L/A) = \_(L/\_W)$$

(P, power, V, voltage, I, current, R, resistance and ρ, resistivity)

The distance between Cu electrodes that supplies the voltage was L, the thickness of graphene film (0.334 nm) was δ, and the width of graphene heater was W. The resistivity was calculated by multiplying the modification factor 4.5324 to sheet resistance. 4.3. Device fabrication functionalizing substrates with SAMs Highly p-doped Si substrates covered with a 300 nm thick Si3N4 were used for the electrical measurement of graphene field effect devices. After treating piranha and rinsing the substrates with DI water, the substrates were placed in a reaction flask. A 20 ml of toluene was added to the reaction flask as well as the silane coupling agent (10 mM). We used two kinds of silanes: γ-APS and OTS for controlling dirac-points. The reaction was performed under an argon atmosphere for 2 h. After reaction was completed, the substrate was baked at 120 ℃ for 10 min, weakly sonicated for 3 min, cleaned with toluene and

then dried under vacuum medium. The graphene film on PSAF was transferred to the prepared substrates and PSAF was carefully pilled off from the graphene film. Cr/Au (5 nm/30 nm) electrode were thermally deposited using pre-patterned stensile mask. Graphene channels were isolated through electron beam lithography and O2 plasma. Before measuring the electrical properties of the graphene device, thermal annealing was carried out at 300 ℃ for 1 h under Ar/H2 gas to remove the unnecessary impurities on graphene surface.

Characterization

An infrared camera (FLIR T650sc) was used to measure the temperature gradient of the graphene films. The sheet resistance was measured using a 4-probe with a nanovoltmeter (Keithley 6221, 2182A) and the Van der Pauw method was applied. The electrical properties were measured by Agilent 2602. Constant 10 mV voltage was applied from source to drain during the measurement. The Raman spectra were recorded using Renishaw Invia Raman Microscope with 1 mW 514 nm Ar laser with the spot size of 2 μm.

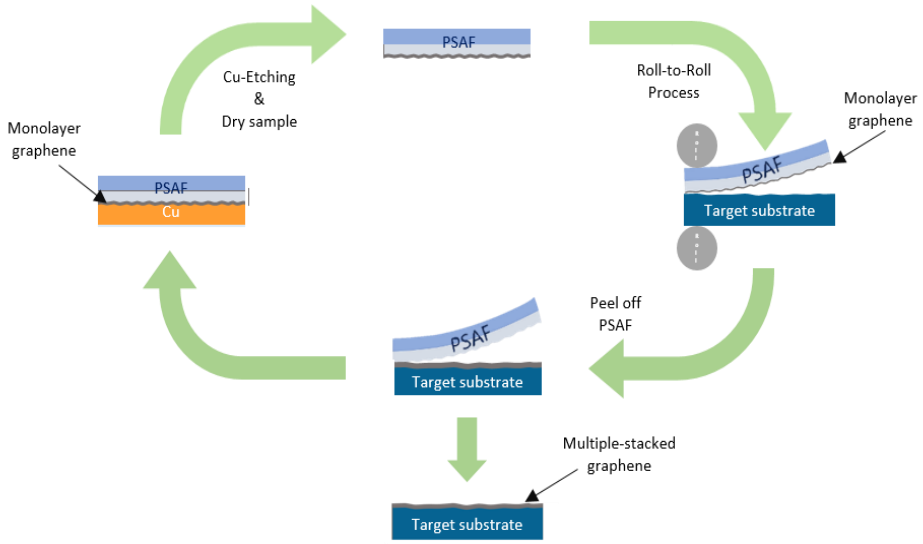

Figure S1. A schematic illustration on the fabrication processes of the graphene on a target substrate based on the use of pressure sensitive adhesive films (PSAFs).

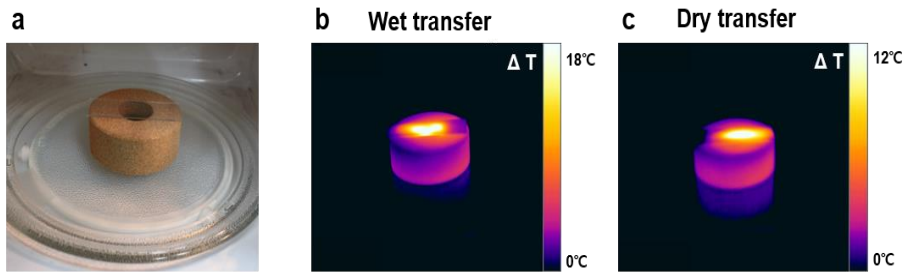

Figure S2. Comparison on the heat-generation properties between dry-transferred and wet-transferred graphene films. (a) An actual photograph image of the graphene films transferred on a slide glass. (b,c) Infrared images showing the EM-heating of wet-transferred and dry-transferred graphene films after irradiating 70 W microwaves for 10 second, respectively.

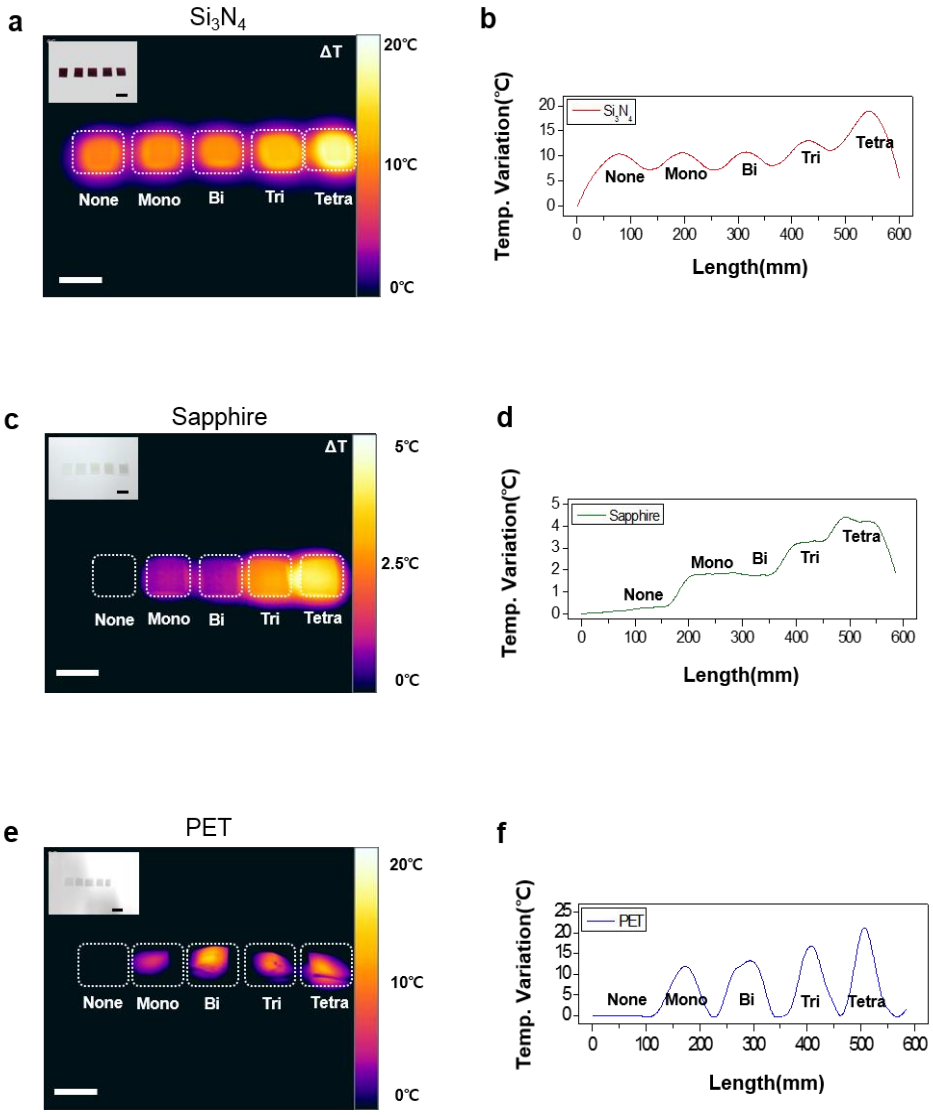

Figure S3. Comparison between the EM heating of graphene on various substrates. (a, c and e) Infrared images of the graphene heaters transferred on Si3N4, PET, sapphire and SiO2/Si substrates, respectively. The inset images are the corresponding photograph images. Scale bars, 1 cm. (b, d and f) Temperature profiles corresponding to a, c and e, respectively.

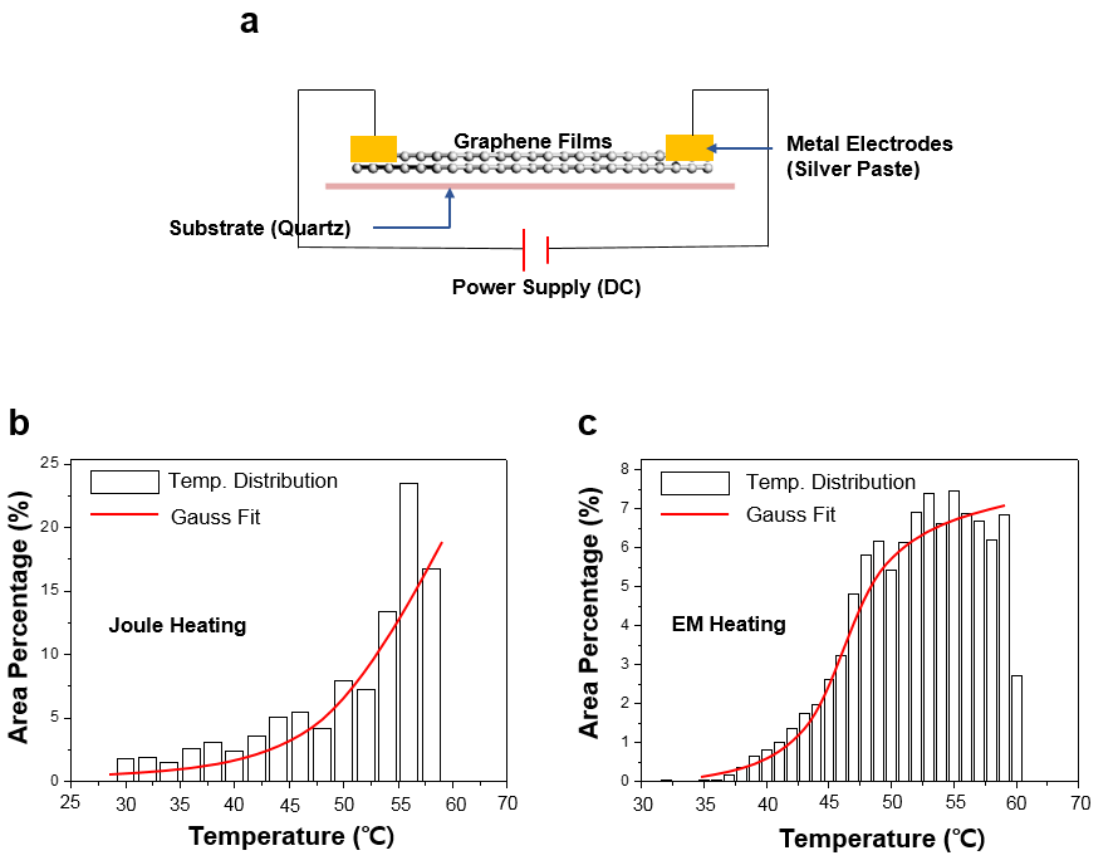

Figure S4. (a) A schematic structure of the Joule-heating type graphene heater. (b, c) Temperature distribution of the Joule heater and the EM heater with 4-layer graphene films working at 70 W, respectively

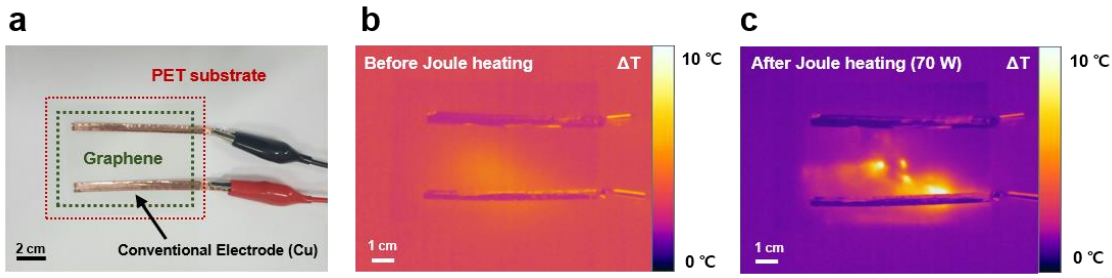

Figure S5. (a) Optical and (b,c) IR photographs showing the Joule heating of monolayer graphene on a PET substrate.

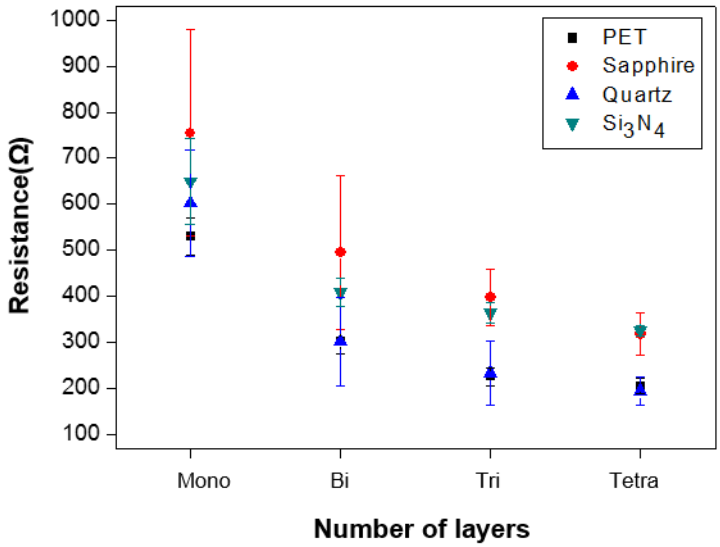

Figure S6. Comparison of sheet reistance depending on the number of graphene layers and substrate types.

3.5 REFERENCES

1. Novoselov, K. S.; Geim, A. K.; Morozov, S. V.; Jiang, D.; Zhang, Y.; Dubonos, S. V.; Grigorieva, I. V. and Firsov, A. A. Electric field effect in atomically thin carbon films *Science* **2004**, 306, 666–9
2. Geim, A. K. and Novoselov, K. S. The rise of graphene *Nat. Mater*. **2007**, 6, 183–91
3. Bolotin, K. I.; Sikes, K. J.; Jiang, Z.; Klima, M.; Fudenberg, G.; Hone, J.; Kim, P. and Stormer, H. L. Ultrahigh electron mobility in suspended graphene *Solid State Commun.* **2008**, 146, 351–5
4. Roche, S. et al Graphene spintronics: the European Flagship perspective *2D Mater.* **2015**, 2
5. Lee, C; Wei, X. D.; Kysar, J. W.; and Hone, J. Measurement of the elastic properties and intrinsic strength of monolayer graphene *Science* **2008**, 321, 385–8
6. Lee, Y.; Bae, S.; Jang, H.; Jang, S.; Zhu, S. E.; Sim, S. H.; Song, Y. I.; Hong, B. H. and Ahn, J. H. Wafer-scale synthesis and transfer of graphene films *Nano Lett.* **2010**, 10, 490–3
7. Bao, Q. L. and Loh, K. P. Graphene photonics, plasmonics, and broadband optoelectronic devices *ACS Nano* **2012**, 6, 3677–94
8. Kim, Y. D. et al Bright visible light emission from graphene *Nat. Nanotechnol.* **2015**, 10, 676–81
9. Elias, D. C. et al Control of graphene's properties by reversible

hydrogenation: evidence for graphane *Science* **2009**, 323, 610–3

10. Wang, X. R.; Li, X. L.; Zhang, L.; Yoon, Y.; Weber, P. K.; Wang, H. L.; Guo, J. and Dai, H. J. N-doping of graphene through electrothermal reactions with ammonia *Science* **2009**, 324, 768–71
11. Parobek, D and Liu, H. T. Wettability of graphene *2D Mater.* **2015**, 2
12. Kim, Y. J.; Kim, Y.; Novoselov, K. and Hong, B. H. Engineering electrical properties of graphene: chemical approaches *2D Mater.* **2015**, 2
13. Tarasov, A.; Tsai, M. Y.; Flynn, E. M.; Joiner, C. A.; Taylor, R. C. and Vogel, E. M. Gold-coated graphene field-effect transistors for quantitative analysis of protein-antibody interactions *2D Mater.* **2015**, 2
14. Blaschke, B. M.; Lottner, M.; Drieschner, S.; Calia, A. B.; Stoiber, K.; Rousseau, L,; Lissourges, G. and Garrido, J. A. Flexible graphene transistors for recording cell action potentials *2D Mater.* **2016**, 3
15. Huang, X. J.; Leng, T.; Chang, K. H.; Chen, J. C.; Novoselov, K. S. and Hu, Z. R. Graphene radio frequency and microwave passive components for low cost wearable electronics *2D Mater.* **2016**, 3
16. Kim, J. et al Engineering structures and functions of mesenchymal stem cells by suspended large-area graphene nanopatterns *2D Mater.* **2016**, 3
17. Koerbitzer, B.; Krauss, P.; Nick, C.; Yadav, S.; Schneider, J. J. and Thielemann, C. Graphene electrodes forstimulation of neuronal cells *2D Mater.* **2016**, 3
18. Muzi, L. et al Examiningthe impact of multi-layer graphene using cellular and amphibian models *2D Mater.* **2016**, 3

19. Yang, C. S. et al Enhancing gas sensing properties of graphene by using a nanoporous substrate *2D Mater.* **2016**, 3

20. Seol, J. H. et al Two-dimensional phonon transport in supported graphene *Science* **2010**, 328 213–6

21. Balandin, A. A. Thermal properties of graphene and nanostructured carbon materials *Nat. Mater.* **2011**, 10, 569–81

22. Kim, K. S.; Zhao, Y.; Jang, H.; Lee, S. Y.; Kim, J. M.; Kim, K. S.; Ahn, J. H.; Kim, P.; Choi, J. Y. and Hong, B. H. Large-scale pattern growth of graphene films for stretchable transparent electrodes *Nature* **2009**, 457, 706–10

23. Bae, S. et al Roll-to-roll production of 30 inch graphene films for transparent electrodes *Nat. Nanotechnol.* **2010**, 5, 574–8

24. Kang, J.; Kim, H.; Kim, K. S.; Lee, S. K.; Bae, S.; Ahn, J. H.; Kim, Y. J.; Choi, J. B. and Hong, B. H. High-performance graphenebased transparent flexible heaters *Nano Lett.* **2011**, 11, 5154–8

25. Kumar, A. and Zhou, C. W. The race to replace tin-doped indium oxide: which material will win *ACS Nano* **2010**, 4, 11–4

26. Hecht, D. S.; Hu, L. B. and Irvin, G. Emerging transparent electrodes based on thin films of carbon nanotubes, graphene, and metallic nanostructures *Adv. Mater.* **2011**, 23, 1482–513

27. Yoon, Y. H.; Song, J. W.; Kim, D.; Kim, J.; Park, J. K.; Oh, S. K. and Han, C. S. Transparent film heater using single-walled carbon nanotubes *Adv. Mater.* **2007**, 19, 4284

28. De, S. and Coleman, J. N. Are there fundamental limitations on the sheet resistance and transmittance of thin graphene films *ACS Nano* **2010**, 4, 2713–20

29. Xia, F. N.; Perebeinos, V.; Lin, Y. M.; Wu, Y. Q. and Avouris, P. The origins and limits of metal-graphene junction resistance Nat. *Nanotechnol.* **2011**, 6, 179–84

30. Hong, S. K.; Kim, K. Y.; Kim, T. Y.; Kim, J. H.; Park, S. W.; Kim, J. H. and Cho, B. J. Electromagnetic interference shielding effectiveness of monolayer graphene *Nanotechnology* **2012**, 23

31. Levendorf, M. P.; Ruiz-Vargas, C. S.; Garg, S. and Park, J. Transfer-free batch fabrication of single layer graphene transistors *Nano Lett.* **2009**, 9, 4479–83

32. Kim, S. J. et al Ultraclean patterned transfer of singlelayer graphene by recyclable pressure sensitive adhesive films *Nano Lett.* **2015**, 15, 3236–40

33. Kim, K. H.; Cho, K. M.; Kim, D. W.; Kim, S. J.; Choi, J.; Bae, S. J.; Park, S. and Jung, H. T. The role of layer-controlled graphene for tunable microwave heating and its applications to the synthesis of inorganic thin films *ACS Appl. Mater. Interfaces* **2016**, 8, 5556–62

34. Park, J.; Lee, W. H.; Huh, S.; Sim, S. H.; Kim, S. B.; Cho, K.; Hong, B. H. and Kim, K. S. Work-function engineering of graphene electrodes by self-assembled monolayers for highperformance organic field-effect transistors *J. Phys. Chem. Lett.* **2011**, 2, 841–5

35. Lee, W. H.; Park, J.; Kim, Y.; Kim, K. S.; Hong, B. H. and Cho, K. Control of graphene field-effect transistors by interfacial hydrophobic self-assembled monolayers *Adv. Mater.* **2011**, 23, 3460

36. Kim, Y.; Cho, D. H.; Ryu, S. and Lee, C. Tuning doping and strain in graphene by microwave-induced annealing *Carbon* **2014**, 67, 673–9

Appendix

A. List of Publications

1. Lee, S.; Jo, I.; Kang, S.; Jang, B.; Moon, J.; Park,J. B.; Lee, S.; Rho, S.; Kim, Y.; Hong, B. H. Smart Contact Lenses with Graphene Coating for Electromagnetic Interference Shielding and Dehydration Protection *ACS Nano* **2017**, 11, 5318-5324

2. Kang, S.; Choi, H.; Lee, S. B.; Park, S. C.; Park, J. B.; Lee, S.; Kim, Y.; Hong, B. H. Efficient heat generation in large-area graphene films by electromagnetic wave absorption *2D Mater.* **2017**, 4, 025037

국문 초록

탄소 원자가 2 차원 방향으로 육각 격자 구조를 이루고 있는 그래핀은 뛰어난 기계적, 전기적 특성 뿐 아니라 생체친화적인 재료로 알려져 있다. 뛰어난 전기적 특성 때문에 그래핀은 가볍고 투명하면서도 매우 우수한 전자기 차폐 재질로 활용 될 수 있다. 구조적인 결함이 없는 이상적인 그래핀은 97.8%의 전자기 차폐 특성을 구현 할 수 있다고 보고 되고 있다. 실험적으로는 그래핀을 대면적으로 합성 할 수 있는 CVD 법으로 제작 한 그래핀에서 모노레이어 기준으로 40%의 전자기 차폐 효과를 얻을 수 있고, 이는 단위 두께로 환산 시 금 박막과 비교하여 7 배에 해당하는 수치이다. 또한 그래핀은 탄소 원자가 육각형의 안정적인 구조로 밀집 해 있어 가스 투과를 차단하는 특성도 가지고 있다. 이렇듯 그래핀은 가볍고, 투명하며 생체친화적인 재질에다 전기적, 기계적 특성이 우수하여, 최근 각광 받고 있는 스마트 일렉트로닉스를 구현하는데 있어 가장 적합한 재료로 판단 된다.

이 논문에서는 CVD 그래핀의 우수한 전자기파 차폐 및 가스 투과 차단 특성을 이용하여, 그래핀이 코팅 된 컨택트 렌즈에서 전자파 차폐

및 안구 건조를 방지하는 효과기 있음을 간접적인 방법으로 증명 하였다. 또한 컨택트 렌즈 위에 그래핀을 정밀 패턴하고 간단한 Micro LED Device 를 제작 함으로서 그래핀을 스마트 컨택트 렌즈를 구현하는데 있어 다양한 용도의 물질로 활용 할 수 있음을 보였다. 또한 CVD 그래핀의 EM 차폐 메커니즘이 그래핀의 높은 전자이동도 및 반자성 특성 때문이라는 것을 증명 하였다. 그래핀의 전자파 차폐 과정에서 열 에너지가 효율적으로 발생되는 것을 이용하여 차량용 방습 히터 등의 어플리케이션으로 활용 가능성을 보였다.

주요어: 그래핀 전자파 차폐, 그래핀 투습 방지, 그래핀 컨택트 렌즈, 그래핀 Heat, 그래핀 반자성

학번: 2014-31011

감사의 글

석사 졸업 10 년 후에 전공까지 바뀌어 다시 학업을 시작 하는 것이 개인적으로 많은 어려움도 있었지만, 주변 지인의 도움으로 4 년 반 동안의 박사 과정을 무사히 마무리 할 수 있었습니다. 이 글을 통해 감사의 마음을 전하고자 합니다.

먼저 지금의 제가 있기까지 낳아 주시고 힘들게 뒷바라지 해 주신 부모님께 감사 드립니다. 정신적인 버팀목이 되어 준 형, 누나에게도 감사 합니다. 나를 믿고 일본에서 먼 타지까지 이주해서 아낌 없이 배려하고 따뜻하게 위로 해주는 영혼의 안식처이자 동반자 미오, 학업 과정 중에 세상에 나와 힘들고 지칠 때 웃음과 희망을 주었던 삶의 원동력이자 나의 보물 아들 준이, 사랑하고 고맙습니다. 그리고 먼 곳에서 격려 해 주신 장모님, 처형 네 식구들 고맙습니다.

박사 과정 동안 그래핀 관련 전공 지식과 연구 활동을 위한 전폭적인 지원뿐만 아니라 아낌없는 지도와 편달을 주신 홍병희 교수님께 깊은 감사의 뜻을 전합니다. 또한 심사를 맡아 주신 장두전 교수님, 남좌민 교수님, 조성표 교수님, 박수범 박사님께 감사 드립니다. 어려웠던

고등학교 시절 희망의 끈을 놓지 않도록 도와 주신 김영붕 선생님, 송복승 선생님 이 글을 빌려 감사의 말씀 전합니다. 학사/석사 과정 늦은 밤까지 같이 고민 해 주시고 열정적으로 가르쳐 주신 시카조노 교수님, 미츠이시 교수님 감사합니다.

학위파견이라는 큰 기회를 주신 홍순국 사장님, 정수화 부사장님, 이영진 담당님께 진심으로 감사 말씀 드립니다. 그리고 회사 업무와 학업을 병행 할 수 있도록 배려 해 주신 이승기 상무님, 박명주 팀장님 감사 드립니다. 마음 편히 학업을 할 수 있도록 항상 응원 해 주었던 파트 원들 고맙습니다. 그리고 저의 회사 생활의 멘토이신 문양식 선배님, 홍승찬 선배님 정말 고맙습니다.

4 년 반 동안 실험실 생활을 하면서 연을 맺은 연구실 구성원들 고맙습니다. 처음 제가 연구실에 발을 디뎠을 때 같은 기계과이고 학위 파견 출신이라 여러모로 의지가 많이 되었던 삼성전기 최태준 수석님, 즐거운 연구실 생활이 되고 연구적으로 많이 모범이 되었던 박수범 선배, 항상 성실하고 진솔한 모습으로 기꺼이 동고동락 해 주었던 쥬짓수 선수 인수, 실험 장비 사용법이나 화학적 이론 지식이 뛰어나서 도움을 많이

받았던 천재 진현이, 실험실 분위기를 활기차게 이끌어 주었던 준희씨, 산기평 과제 수행 시 열성적이고 누구 보다 도 적극적으로 도와줬던 동진이, 보스턴에서 폭설 속에 좋은 추억을 만들어 준 용석이, 배권이, 성채, 그래핀 패터닝 실험에 고군분투 해준 상민이, 그리고 행정 업무로 항상 바쁘지만 웃는 얼굴로 도와 주시는 구은하 선생님, 김유리 선생님 감사합니다.

여전히 고등학교 때나 지금이나 만나면 쓸데 없는 이야기로 스트레스를 풀게 해주는 규성이, 명운이, 현이, 일본 유학 생활을 동고동락 하며 덕분에 즐겁게 보냈던 원보 형, 종현이, 기철이 고맙다.

이 외에도 미처 언급하지 못한 많은 분들의 이름을 모두 되새기지 못해 죄송하며 고마운 마음을 전하며 글을 마칩니다.

2018 년 11 월 25 일